Automating historical centering-minimizing masonry vaulting strategies
Applications to cooperative robotic construction

Bruun, Edvard P.G.; Oval, Robin; Al Asali, Wesam; Gáspár, Orsolya; Paris, Vittorio; Adriaenssens, Sigrid

DOI
10.1016/j.dibe.2024.100516

Publication date
2024

Document Version
Final published version

Published in
Developments in the Built Environment

Developments in the Built Environment 20 (2024) 100516

Contents lists available at ScienceDirect

Developments in the Built Environment

journal homepage: www.sciencedirect.com/journal/developments-in-the-built-environment

Automating historical centering-minimizing masonry vaulting strategies: Applications to cooperative robotic construction

Edvard P.G. Bruun [a,b,*], Robin Oval [b,c], Wesam Al Asali [d], Orsolya Gáspár [e], Vittorio Paris [f], Sigrid Adriaenssens [b]

[a] Bruun Automation Research Lab, School of Civil and Environmental Engineering, Georgia Institute of Technology, United States
[b] Form Finding Lab, Civil and Environmental Engineering Department, Princeton University, United States
[c] Faculty of Civil Engineering & Geosciences, Delft University of Technology, the Netherlands
[d] IE School of Architecture and Design, Spain
[e] Department of Architecture, Pennsylvania State University, United States
[f] Department of Engineering and Applied Sciences, University of Bergamo, Italy

ARTICLE INFO

Keywords:
Masonry
Automation
Assembly
Cooperative
Robot
Vaults
Centering
Scaffold-free

ABSTRACT

This paper investigates the feasibility of adapting ancient historical construction techniques to cooperative robotic assembly methods to minimize centering requirements in masonry vaults. First, an overview of seven historical techniques is presented. Next, a classification framework is introduced to evaluate the automation potential of these methods, identifying the rib network as the most promising candidate. This is followed by two computational case studies on the cooperative robotic construction of planar masonry arches and multi-arch rib networks. These studies evaluated the impact of robotic reachability and support payload on the feasibility of centering-free construction. A conclusion based only on these simulation results is that high-payload fixed robots, in comparison to medium-payload mobile setups, allow for the construction of larger and more complex rib structures. This research is of relevance to architects and engineers interested in using a cooperative robotic fabrication framework to reduce centering in masonry vault construction.

1. Introduction

1.1. Falsework in traditional masonry vault construction

Shells and vaults are efficient structural systems that have the potential to effectively reduce the environmental impact of construction using low-embodied carbon and locally sourced building materials (De Wolf et al., 2016). While these materials (e.g., stone and clay bricks) may have lower strength and tensile capacity, they can be utilized effectively by specifically designing structural forms that prioritize force distribution through compression while minimizing bending and tensile stresses. However, the pursuit of such specifically optimized forms can lead to unique geometries that are tailored to specific boundary conditions and load distributions, necessitating custom falsework to guarantee stability during construction that is not reusable for other projects with different design criteria. Falsework, which includes centering and guidework in the context of masonry construction, encompasses temporary structures used during assembly to provide support for the structure, guide the masons, and are later dismantled and disposed of upon completion of the structure.

The use of falsework in the construction of mechanically efficient shells and vaults poses economic challenges due to its negative impact on masonry labor through increased construction time and costs (Sanders and Thomas, 1991). The use of falsework involves several aspects that contribute to these challenges. Firstly, it requires filling the entire volume below the structural surface, necessitating additional design and planning efforts. Secondly, it takes time to assemble and requires careful decentering to ensure safety. Furthermore, falsework needs to be dismantled while the complete structure covers it, generating waste, especially for unique curved geometries. Numerous studies have emphasized the material costs associated with falsework, reporting that it can range from 15% to 60% of the overall construction cost for concrete casting (Hanna, 1998; Lab, 2007; Ko and Kuo, 2015). In cases involving geometrically complex walls, falsework has been found to account for approximately 60% of the total construction time (García et al., 2018). Even innovative approaches like reusable lightweight

* Corresponding author. Bruun Automation Research Lab, School of Civil and Environmental Engineering, Georgia Institute of Technology, United States.
E-mail address: edvard.bruun@ce.gatech.edu (E.P.G. Bruun).

https://doi.org/10.1016/j.dibe.2024.100516
Received 25 April 2024; Received in revised form 3 August 2024; Accepted 4 August 2024
Available online 10 September 2024

falsework still require a significant amount of material for the temporary structure in proportion to the weight of the masonry structure (Davis et al., 2012), which make the construction process less efficient and potentially less easily automated. Noteworthy examples of falsework usage in free-form brick and stone vaults further underscore its significance in construction, as demonstrated in recent works (López et al., 2014; Rippmann et al., 2016).

Falsework is thus an undesirable feature of constructing shells and vaults and is seen as an extra step towards construction that many building cultures throughout history have endeavored to eliminate. As temporary supporting structures are traditionally made from timber, techniques of minimizing it have historically thrived in arid regions with rich vaulting culture, like the Middle East, Central Asia, and North Africa (Choisy, 1883; Fathy, 1973; Wendland, 2007). Vault builders in these regions employed various design and construction techniques to reduce the reliance on falsework. These techniques include: (1) designing modular components that reuse the same centering (Lancaster, 2009), (2) employing movable centering that slides along the structure as it is being constructed (Lancaster, 2009), and (3) developing construction methods that rely on structural form in tandem with material properties to ensure the self-stability of the structure during construction.

In this paper we will explore the latter, traditional methods that leverage structural mechanics as a function of building form (e.g., leaning arches, squinches, counterweights etc.) and material properties of bonding mortar to minimize centering.

1.2. Research objectives

Motivated by both material constraints, skilled masons have ingeniously devised construction strategies over time, aiming to streamline, simplify, and eliminate the necessity for centering and guidework in the creation of vaulted masonry structures. These historical constraints, rooted in the quest for minimizing material usage, persist into the modern era, forming the focus of our study that endeavors to reduce material usage in response to resource depletion and increased scarcity within the contemporary construction industry.

The principal aim of this research is to investigate the synergy between traditional construction methods and cutting-edge digital fabrication approaches. These contemporary techniques have generally demonstrated the ability to enhance construction productivity, especially in the context of geometrically intricate structures (García et al., 2018). Specifically, the growing adoption of cooperative robotic fabrication setups in the construction industry presents an opportunity to explore novel construction processes that better align with the sustainability goals of a circular economy (Bruun et al., 2024a). Specifically, our focus is on unraveling how historical insights and techniques can be applied to modern cooperative robotic fabrication methods, facilitating the construction of masonry vaults while concurrently reducing dependence on temporary centering structures.

To adequately address this question, we initiate the study by examining and categorizing historical techniques that have minimized the use of falsework. This categorization serves as the basis for selecting a specific method with the potential for automation, tackling the challenges of minimizing temporary centering structures and optimizing material utilization. This selected method is further explored through computational case studies simulating its implementation with different cooperative robotic setups, where the robots collaboratively sequence their actions, alternating between assembly and support roles during construction. By demonstrating the capabilities of contemporary cooperative robotic assembly methods, our study presents an alternative to manual construction for masonry vaults.

1.3. Paper organization

The paper begins with Section 2, an overview and structural analysis of seven historical strategies for the construction of masonry vaults with minimal falsework. This paper does not aim to present a comprehensive academic review on the topic or to narrate in detail the history and application of these strategies, but rather to summarize each from its large body of literature for the sake of high-level comparison and categorization. We therefore rely on secondary data from the existing literature to summarize the different construction strategies, starting with a review of historical origin(s) and a list of notable built examples. We explain how each method achieves its self-supporting characteristic, accompanied by schematic figures illustrating the structural mechanics during the "construction phase" and the resulting "built state".

In Section 3, a classification methodology is introduced, grounded in the self-supporting structural mechanics and primary design parameters described in Section 2, leading to the organization and classification of the seven methods to determine which ones are most readily adaptable to robotic construction techniques. Section 4 outlines two computational case studies aimed at further investigating the rib network construction strategy, identified as the most readily adaptable to robotic construction methods. Following this, the results of these two computational studies are presented, and their significance is discussed in Section 5. The conclusion in Section 6 summarizes the main findings, discusses the potential of automating traditional masonry construction techniques, and presents limitations of the current research as the basis for future work.

1.4. Previous work and current research contributions

The use of cooperating robots to minimize scaffolding in masonry construction has been exemplified in prior work by the authors. In the centering-free construction of the LightVault we demonstrated the construction of a doubly-curved masonry vault without external falsework, employing two cooperating robotic arms (Parascho et al., 2020, 2021; Han et al., 2020; Bruun et al., 2021). While these preceding papers are pivotal precursors to the current study, their scope is limited, primarily focusing on the physical construction of a single vault geometry. In the current paper, computational simulations are used to explore a broader design space.

The primary research contribution of this paper lies in examining the feasibility and effectiveness of the support/place cooperative robotic construction methodology developed in the LightVault project when applied to various construction methods and arch geometries. The computational studies presented herein build upon this established methodology by investigating a broader array of arch geometries and exploring the impact of different robotic setups, ranging from mobile to fixed configurations. The objective is to delineate critical geometric constraints, structural limitations, and associated trade-offs when employing multiple cooperating robots in diverse configurations for scaffold-free construction.

The following is a summary of our principal contributions.

1. Analysis of historical construction strategies aimed at reducing or eliminating the need for falsework in masonry vault assembly, categorized based on a set of qualitative structural metrics developed by the authors.
2. Simulation of the construction of 48 distinct planar masonry arch geometries using either a two-robot mobile or fixed robot setup to elucidate the limitations of different cooperative robotic configurations.
3. Simulation of the cooperative robotic assembly of multi-arch rib networks using a three-robot fixed setup.

2. Historical overview and structural analysis of falsework-minimizing construction strategies

This section presents an overview and structural analysis of seven historical construction strategies that have been used to reduce, or eliminate, the necessary falsework typically needed for the assembly of

masonry vaults. For each construction strategy, we highlight its more recent applications in both industry and academia for the construction of masonry vaults and concrete shells. For a comprehensive overview, Fig. 8 visually summarizes all seven construction methods, depicting their structural mechanics and the earliest recorded instances of their use.

2.1. Corbelling

Corbelling techniques, with roots dating to Sumerian burial vaults around 3rd or 4th millennium BCE (Woolley, 1929), have evolved into various forms influenced by materials and regions. Here, "corbelling" broadly refers to all these variations, characterized by horizontally layered cantilevered stones or bricks, relying on counterweight to prevent overturning.

In some cases, dry joints were employed where the structure's own weight provided the necessary counterweight. In other cases, external infill material was used as an alternative counterweight (see Fig. 1). The assembly process itself varied, with some structures following a spiral sequence (Mecca and Dipasquale, 2009) while others were constructed with horizontal rings (Roberti and Spina, 2001). The construction of arches and domes relied on careful stacking of the building blocks, adhering to precise geometric assembly sequence principles (Benvenuto and Corradi, 1987; Fraddosio et al., 2019). These principles, derived from empirical observation, would consider the proportions of the building blocks and the curvature of the dome under construction (Cappai, 2003).

Corbelling can still be seen in villages around the Mediterranean Sea, in Beehive villages in Syria (Copeland, 1955; Mecca and Dipasquale, 2009), Trulli villages (Fraddosio et al., 2019) or Nuraghe buildings in Italy (Roberti and Spina, 2001; Allen, 1979). Recently, the corbelling approach was adapted for concrete 3D printing, allowing for cantilevered construction by progressively offsetting horizontal layers (Carneau et al., 2020).

2.2. Pitched vaulting

Pitched vaulting has its origins in the Old Kingdom of Egypt period, specifically in Nubia, a region of Upper Egypt encompassing present-day South Egypt and North Sudan, dating back to approximately 2700-2100 BCE (von Pilgrim et al., 2011). Nubian vaults are constructed using thin, inclined arches that are assembled leaning against one another, relying on the friction and adhesion between adjacent arches.

For a barrel vault, the assembly process begins with a supporting wall, which is essential for providing stability and support to the initial arch. Subsequently, a series of oblique arches are added, following a specific pattern (see Fig. 2). These arches can be combined in various orientations to create different vault designs.

A variation of the pitched technique involves utilizing the corners between walls to construct pendentive vaults instead of barrel vaults. Pendentive vaults using the pitched technique originated in Mesopotamia, with archaeological evidence dating as far back as 1200 BCE in Tell Al-Rimah, located in modern-day Iraq (Oates, 1970).

The technique of pitched vaulting subsequently found its way to various regions across Africa (Vitti, 2021), the Middle East (Vitti, 2021), and the Mediterranean area (Choisy, 1883). The architectural styles of ancient Egypt and Mesopotamia heavily influenced later vaulting strategies, particularly during the Greek and Byzantine periods, where fired bricks were employed instead of raw mud bricks. Numerous examples of pitched vaulting could be found throughout Europe, particularly in contemporary Greece and Turkey, with many of these structures still standing in the 19th century when documented by Auguste Choisy (Choisy, 1871; Huerta, 2009). The arches are laid out in a manner that spans the shortest distance between supports, whether they are walls, columns, temporary centering on the periphery, or previously constructed arches.

Examples of pitched vaulting, incorporating squinch and pendentive forms, can be found in various locations. Notable instances include the houses at Ephesus and a theater at Nysa, both situated in Turkey (Lancaster, 2015a). Additionally, the Tabriz Bazaar in Iran, which was constructed around the 13th century CE and is still in use today (Petralla, 2013). In Upper Egypt, examples of pitched vaulting can be traced back to the Roman era (Rossi and Fiorillo, 2020) and even as recent as the early 20th century (Zabrana, 2018), highlighting its longevity in the region. A variation of pitched vaulting, employing a staggered pattern of fan-shaped curved squinches, has been utilized in structures such as the Palace of Diocletian in Spalatro, Dalmatia (currently Split, Croatia), circa 305 CE, and the Church of Saint Demetrios in Thessaloniki, Greece, dating back to the 5th century CE (Lancaster, 2015a; Choisy, 1883; Adam, 1764).

This construction technique is still an active vernacular craft today in some countries. In Egypt, the revival work of Hassan Fathy has contributed to its continued practice (Fathy, 1973). The Auroville Earth

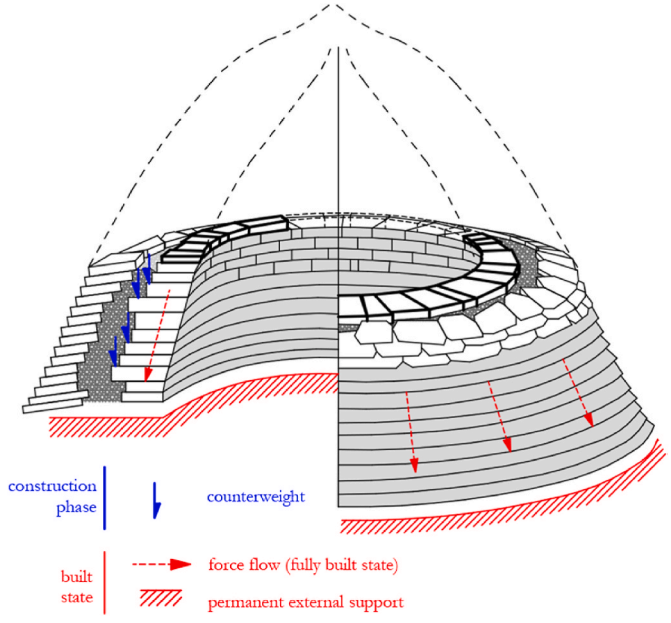

Fig. 1. Corbelling structural schematic in the construction of a drystone hut showing the counterweight force necessary to balance cantilevered layers during construction (adapted from (Lassure, 2009)).

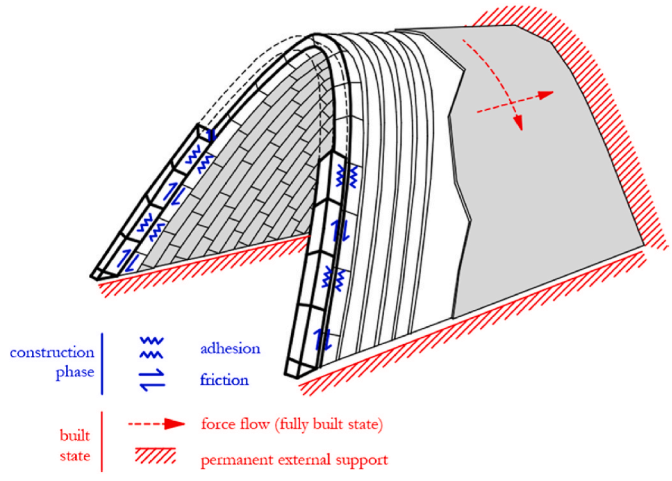

Fig. 2. Pitched vaulting structural schematic for the construction of a barrel vault showing the adhesion and friction in the inclined layers during construction.

Institute in India has also demonstrated pitched vaulting in their architectural work (Auroville Earth Institute et al., 2022). In Mexico, Alfonso Ramirez Ponce, along with builders like Fernando Lopez Carmona, have demonstrated this building technique in projects such as Carmona's own house in Queretaro and the Nuestra Senora del Rosario Church (Ramírez Ponce, 2012; Ramírez et al., 2015; Guzmán et al., 2010). Pitched vaulting has also found applications in concrete and earth 3D printing to avoid the use of supports (Motamedi et al., 2022).

2.3. Interlocking voussoirs

The technique of interlocking voussoirs involves the use of specially designed building units that can interlock and provide mutual support, thus enabling the construction of cantilevered structures without scaffolding. There are two primary strategies employed: the nesting of adjacent pairs of voussoirs in a single direction (i.e., planar construction) or the reciprocal interlocking of groups of voussoirs in all directions (i.e., surface construction).

A historical example of interlocking blocks with jagged edges, enabling the construction of masonry arches, was uncovered in a Giza tomb dating back to 2300 BCE (Fisher, 1924). From the 3rd century BCE until the Roman era, another application of interlocking construction was observed with the use of clay tubes with tapered profiles. These tubes were employed to construct vaults arch by arch, where each tube could nest within its neighbor, thus resulting in a more rigid connection (Lancaster, 2015b) (see Fig. 3). In 1699, Joseph Abeille patented a reciprocal system that utilized flat stone slabs with modular voussoirs based on tetrahedra. This system involved inclined interfaces between the blocks, where one pair of blocks provided support while being supported by another pair (Gallon, 1735). However, the implementation of such an interlocking strategy required the use of intricate block shapes and expertise in the art of stone stereotomy.

Drawing inspiration from the Roman approach, the utilization of ceramic fuses and tubes experienced a revival in the 20th century for construction purposes in India (Jalia, 2017). Anupama Kundoo further pushed the boundaries of experimentation by incorporating cylindrical roof structures through the implementation of tube vaulting in the Wall House situated in Auroville (Kundoo, 2014). Beyond practical applications, experimental research has delved into various facets of interlocking construction. Investigations have encompassed diverse module shapes (Dyskin et al., 2003), their application into curved structures (Brocato and Mondardini, 2012), the impact of patterns on mechanical behavior (Fantin et al., 2018), the kinematics necessary for centering-free assembly in curved vaults with potential applications in robotic implementation (Loing et al., 2020), as well as endeavors to generalize achievable masonry surfaces (Wang et al., 2019) and blocks (Akleman et al., 2020).

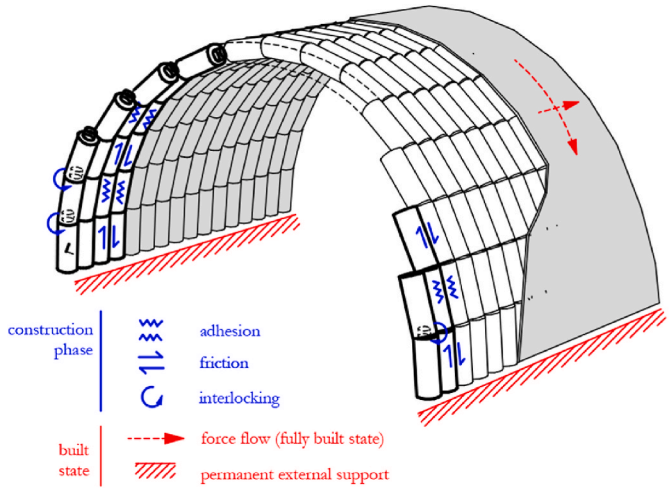

Fig. 3. Interlocking voussoirs structural schematic for the construction of a barrel vault showing the interlocking between adjacent tapered tubes in a planar arch and the friction and adhesion between adjacent arches.

2.4. Thin-tile vaulting

Thin-tile vaulting (also called Catalan, Guastavino, or timbrel vaulting) is a technique that flourished in the Western Mediterranean region, concentrated in Spain and South France with many examples found in the medieval architecture of the region (Ochsendorf, 2013). The construction strategy relies on a fast-setting mortar to build an initial layer of hollow tiles without a supporting structure (López et al., 2016) (see Fig. 4). A light guidework, usually made of flexible rods fixed at the end of poles, is necessary to allow the masons to control and correct the geometry during assembly. The first layer of tiles then provides support to additional layers with courses in different directions.

The earliest known instance of thin-tile vaulting can be found in Morocco, specifically in the dome of the Qubba al-Barudiyyin in Marrakech, constructed in 1070 (Ochsendorf, 2013). In Europe, one of the oldest thin-tile vaults discovered to date is in the Hospital of Santa Maria in Lleida, Catalonia, built in 1352 (Al et al., 2021). Since then, this technique has continued to be used in Spain and played a significant role in the development of Catalan Modernisme during the late 19th century, as seen in the architectural works of Antoni Gaudi and Josep Puig i Cadafaalch (Al et al., 2021). Rafael Guastavino introduced this technique to the United States in the 19th century, having utilized it in the construction of the Batlló Factory in Barcelona in 1868 (Collins, 1968). Numerous examples of thin-tile vaulting can still be found in the United States today, such as the market situated beneath the Queensboro Bridge in New York City, built in 1909 (Ochsendorf, 2013).

The craft of tile vaulting has maintained its popularity in modern times, with notable examples of construction found in Cuba, Tunisia, France, and Spain (Al et al., 2021). This technique has garnered attention since the early 2000s due to its association with minimal waste and material usage. As a result, projects utilizing tile vaulting have emerged both within its historical context and beyond. Noteworthy examples include the Pines Calyx Center in the UK (Ramage, 2007), as well as the Light Earth Design projects in South Africa and Rwanda (Ramage et al., 2019). In the academic context, researchers have explored the application of computational methods to design innovative vault forms that can be constructed using the thin-tile vaulting technique (Davis et al., 2012; López et al., 2014). Additionally, there have been investigations into novel approaches for the fabrication and construction of such vaults (Al et al., 2021).

2.5. Rib network

The evolution of ribbed domes and vaults can be traced through two

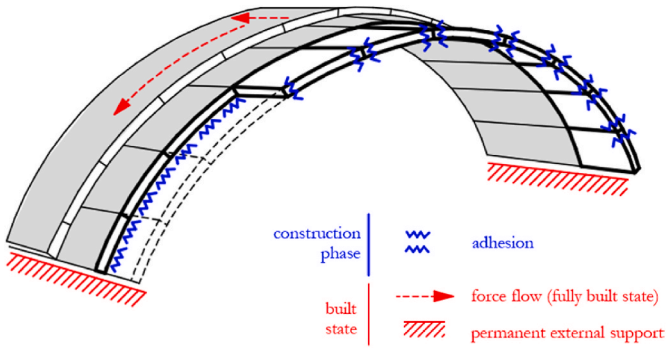

Fig. 4. Thin-tile vaulting structural schematic for the construction of a barrel vault showing the adhesion between bricks in the first layer of hollow tiles.

architectural periods. Firstly, Islamic-Moorish architecture of the Omeyyades from the 7th to the 11th century (Arce, 2003; Fuentes and Huerta, 2010; Alkadi, 2017). Subsequently, in the Romanesque-Gothic architecture from the 11th to the 16th century (Fitchen, 1981; Fuentes and Huerta, 2015).

While the structural benefits of ribs in completed vaults remain a topic of debate (Fitchen, 1981), part of their value lies in establishing a structural hierarchy that can be leveraged during construction. Typically, the ribs are erected first, acting as support for, and simplifying the subsequent placement of, the remaining vault surface placed over the reduced spans between adjacent ribs (see Fig. 5). Although not strictly centering-free, this construction technique significantly minimizes the overall weight of external supporting structure required throughout the entire vault. Only the ribs require traditional heavy centering, while the support structure for the remaining vault surface can be lighter. For instance, this can take the form of a lagging unit directly supported by the ribs (Fitchen, 1981). Alternatively, other centering-free strategies can be employed to place the bricks between the ribs, potentially eliminating the necessity for additional support altogether.

This construction method is evident in the Al-Ukhaidir Fortress in Iraq, constructed in 775, which used prefabricated plaster arches as part of its construction (Reuther, 1912). Once the rib network was completed, the remaining vault was built without additional centering by spanning between the ribs using skewed brick courses, reminiscent of the pitched vaulting approach. Later during the late Gothic period, Central European architecture witnessed the development of diamond vaults, characterized by intricate rib patterns and built with this technique (Talaverano et al., 2012). An example is the Albrechtsburg Castle in Meissen, Germany, which was completed in 1495 (Opačić, 2005).

In recent years, there has been a resurgence of interest among architects and designers to reinterpret and adapt the concept of ribbed vaults to contemporary construction methods. This exploration has led to innovative approaches that blend traditional techniques with modern materials and technologies. One example is the work of Gabinete de Arquitectura, which developed a technique for building lattice brick vaults as a model for low-cost construction (Gabinete de and Arquitectura, 2015; Aravena, 2016). This modern interpretation of ribbed vault construction combines the use of traditional brick materials with a lattice-like structure. Another modern example is seen in the concept of Ribbed Tile Vaulting, which was developed through two design-build workshops that brought together architects, engineers, and craftsmen to explore the potential of using tiles as the main building material for ribbed vaults (Block et al., 2017). In the context of robotic assembly, cooperating robots have been used to assemble a branching rib network made of custom foam blocks (Wu and Kilian, 2018, 2020) and the central arch of the LightVault glass-brick vault (Parascho et al., 2021).

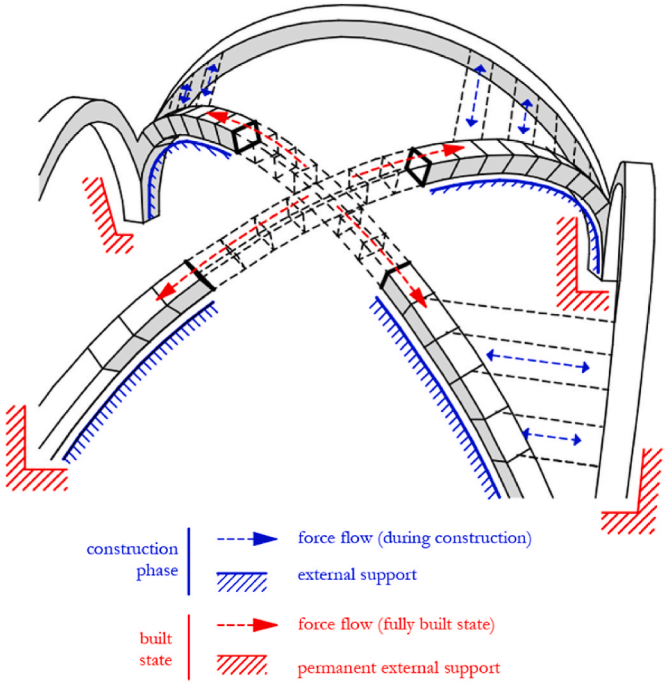

Fig. 5. Rib network structural schematic for the construction of a vault showing the external support that is initially required to construct the ribs followed by the ribs acting as support for the remaining structure spanning between them.

2.6. Herringbone pattern

Herringbone patterns are characterized by the arrangement of vertical bricks within standard horizontal brick courses creating loxodromic curves on the dome surface. While these patterns are commonly employed for decorative purposes, they also offer a solution for centering-free construction through the construction of self-supporting sub-structures known as plate-bandes. These sub-structures can be thought of as arches spanning in the direction of the horizontal coursing, which become stable only when clamped between the vertical bricks that make up the loxodromic curves (Paris et al., 2020). These vertical bricks are locked into the previously completed horizontal layer, which allows them to function as cantilevers that can be used as fixed supports for the next horizontal plate-bande spanning between them (see Fig. 6).

Historically, herringbone patterns have been employed in the construction of Persian domes, such as the Ardestan Mosque (1088), the Taj-Ol-Molk Dome in the Jameh Mosque of Isfahan (1158) in Iran (Sadeqi et al., 2019), as well as the Great Mosque in Eski Malatya (1224) in Turkey. An alternative to the traditional herringbone pattern is evident in the 46m-span Soltaniyeh Dome, built in Iran in 1312, which utilizes straight ribs and skewed brick courses instead of the typical skewed loxodromes and straight courses seen in conventional herringbone construction (Sanpaolesi, 1972; Brambilla, 2012). The 44m-span Santa Maria del Fiore Cathedral in Florence, constructed by Brunelleschi in 1436, also highlights the use of herringbone patterns (Mainstone, 1969; Askarov, 2004).

The herringbone technique is not commonly employed in contemporary construction except for verification tests and structures built for research purposes. However, a modified version of this technique has gained popularity among builders of pitched vaults in Mexico and Egypt. In these vaults, the herringbone pattern is used decoratively and referred to as “costuras” or seams. An excellent example highlighting the

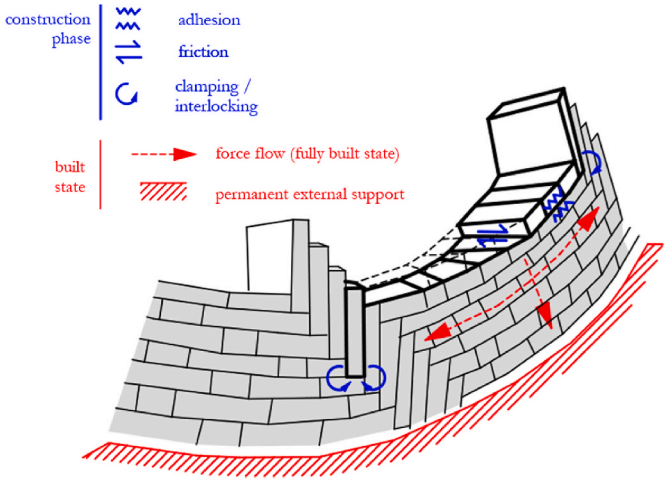

Fig. 6. Herringbone structural schematic for the construction of a dome segment showing how a plate-bande (i.e., horizontal arch) is clamped between two vertical bricks that are locked in place by the previous brick course.

decorative herringbone pattern can be observed in the Nuevo Mercado, Cunduacán, Mexico.

2.7. Cable system

The term "cable system" encompasses a wide range of methods that utilize external cables and counterweights to balance destabilizing forces during construction. Specifically in the context of spanning masonry structures, a cable system can take the form of hanging weights that apply gravity-induced compressive forces, acting as pre-stress to resist overturning for partial arches or curved surfaces (see Fig. 7). While not strictly centering-free, implementing a cable system in this manner eliminates the need for extensive falsework typically required. Furthermore, this technology offers advantages such as straightforward installation, targeted usage (i.e., can be moved to where required), and positioning outside the covered span, allowing unimpeded space below the structure for construction activities (Fitchen, 1981). Cable systems have been observed in the construction of Gothic cathedrals, and were also employed in Vienna, Austria during the early 19th century (Lassaulx, 1829; Lassaulx and Whewell, 1831; Whewell, 1830).

In modern-day construction, counterweight cable systems are primarily seen in the construction of "flying-bird" type steel and concrete bridges, which involve connecting two cantilevering half arches supported from abutments. However, there are a few examples of their application in masonry construction as well. One such example is the Arch-Lock system, used for constructing small-span masonry arches and barrel vaults. This system utilizes cables anchored to counterweight blocks that are required for stability until the arch is fully constructed and becomes self-supporting (Drew, 2017). Additionally, a cable-based construction strategy has been studied for complex free-form masonry vaults, demonstrating a small-scale implementation with a search algorithm to minimize the number of cables and connection steps required (Deuss et al., 2014). Lastly, the FlexiArch system enables the assembly of prefabricated block arches, which are supported from a cable attached to a crane directly on site (Gupta et al., 2016).

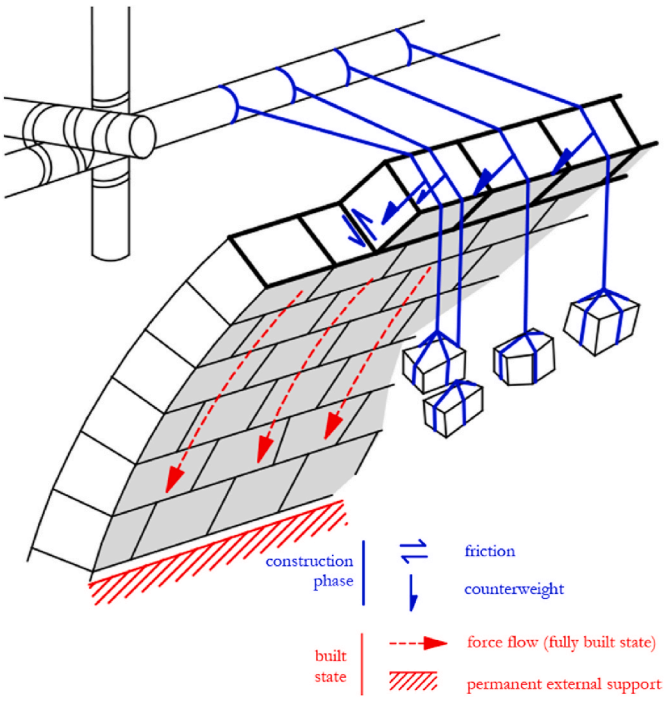

Fig. 7. Cable system structural schematic for a masonry arch showing how suspended weights can be used induce compressive forces into the structure to resist overturning.

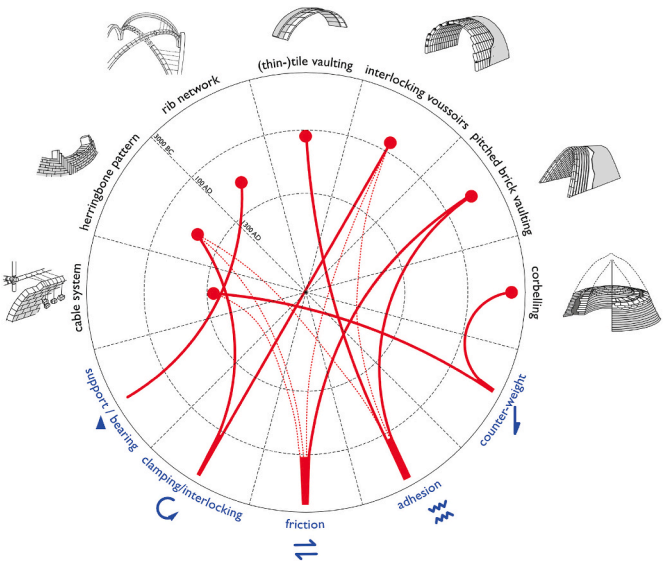

Fig. 8. A diagram showcasing the relevant primary and secondary structural actions (solid and dashed red lines respectively) and indicating the first documented occurrence for each of the seven falsework-minimizing construction methods (newer towards the center of the circle).

3. Classification of construction strategies

In Section 2, we examined seven historical strategies utilized for constructing centering-free masonry vaults, spanning diverse geographical, temporal, and vernacular contexts. As discussed, these strategies exhibit significant variation in their fundamental structural function and physical execution. Consequently, our objective in the subsequent section is to establish a common classification system to facilitate a comparative evaluation between these methods. The classification system we introduce is qualitative in nature and centers around how each method achieves its centering-minimizing quality within its particular structural system. We employ two user-defined structural criteria to categorize each method, including.

1. Self-supporting structural mechanic(s)
2. Primary structural design parameter(s)

The two criteria are discussed further in Sections 3.1 and 3.2 and the results of this classification are summarized in Table 1 with the relative classification of the methods discussed in Section 3.3 then making conclusions about their adaptability to robotic assembly in Sections 3.4 and 3.5.

3.1. Self-supporting structural mechanic

The first criterion is based on whether the self-supporting functionality of the system originates from an internal, external, or hybrid structural mechanic (see "construction phase" forces shown for each method in Fig. 8).

3.1.1. Internal structural mechanic

Where self-support is achieved through friction, adhesion, interlocking, clamping, counter-weight between features that are part of the masonry structure itself (i.e., bricks, courses, sub-structures etc.). For example.

- In dry-stacked corbelling construction, the overturning counterweight effect generated by the self-weight of subsequent brick layers.
- In pitched vaulting, the internal friction and adhesion between adjacent inclined brick arches.

Table 1
Classification of construction methods based on structural support mechanic and design parameters.

Strategy	Support Mechanic	Design Parameter(s)	Description
corbelling	INTERNAL (counterweight)	GLOBAL (assembly hierarchy tessellation geometry)	sequencing bricks or infill as counterweight
pitched vaulting	INTERNAL (friction/adhesion)	LOCAL (tessellation geometry material properties)	inclining arches to rest on adjacent layer
interlocking voussoirs	INTERNAL (interlocking/friction/adhesion)	LOCAL (tessellation geometry assembly hierarchy)	shaping blocks to interlock with neighbors
thin-tile vaulting	INTERNAL (adhesion)	LOCAL (material properties)	using fast-setting mortar and light tiles as initial layer
rib network	HYBRID (support/bearing)	GLOBAL (assembly hierarchy equipment technology)	building ribs first to support the remaining vault
herringbone pattern	INTERNAL (clamping/friction/adhesion)	GLOBAL (assembly hierarchy)	clamping horizontal arches with transverse bricks
cable system	EXTERNAL (counterweight/friction)	GLOBAL (equipment technology)	counteracting overturning with counterweight

- In interlocking voussoirs, the interlocking nature of the voussoirs and their friction with adjacent blocks.
- In herringbone pattern construction, the clamping of horizontal brick arches between vertical loxodrome bricks.

3.1.2. External structural mechanic

Where self-support is achieved through counter-weight or support from a system that is external to the masonry structure itself. For example.

- In cable system construction, the temporary prestress induced into a partially constructed structure to counteract overturning.
- In corbelling construction using infill, the overturning counterweight effect generated both by the self-weight of the infill combined with the subsequent brick layers. Although initially external, the infill material remains integral to the completed structure.

3.1.3. Hybrid structural mechanic

Where self-support is achieved through a combination of internal and external structural mechanics. For example.

- In rib network construction, the external bearing support initially required to construct the ribs. Once the ribs are completed they function as stay-in-place formwork and internal bearing support for the rest of the vault surface spanning between adjacent ribs.

3.2. Primary structural design parameter

The second criterion is identifying whether the self-supporting nature of the method is primarily based on a local-level (i.e., bottom-up) or global-level (i.e., top-down) design parameter.

3.2.1. Local design parameter

Examples of local (i.e., bottom-up) design parameters are tesselation geometry and material properties.

Tessellation geometry refers to where self-support is achieved through the interplay of individual block shapes and the orientation and placement of their interfaces with neighboring blocks at a local level. For example.

- In pitched vaulting, the inclination angle of bricks in adjacent planar arches that are built and supported sequentially along the length of the vault.
- In corbelling, the placement of horizontal seams and the shaping of individual blocks as counterweight for adjacent courses.
- In tube-based voussoir systems, the shaping of individual interlocking hollow tubes to construct unsupported cantilevers.

Material properties refers to where self-support is achieved primarily by relying on the local material properties of either the bricks or mortar. For example.

- In pitched vaulting, the mortar must achieve the proper roughness thus providing adequate friction between adjacent inclined brick courses.
- In thin-tile vaulting, the mortar must set quickly enough to provide adequate moment resistance to cantilevering bricks in the first layer of the vault.

3.2.2. Global design parameter

Examples of global (i.e., top-down) design parameters are assembly hierarchy and equipment technology.

Assembly hierarchy refers to where self-support is a function of how global-level structural features are sequenced during construction. Rather than relying on the connection behavior of individual blocks, stability is based on the interactions between regions or groups of

blocks. For example.

- In rib network construction, a series of connected ribs must first be constructed and then function as a support system for the remaining vault surface.
- In herringbone pattern construction, pairs of transverse loxodrome bricks must first be placed to act as supports for the horizontal arch bricks to span between.
- In some interlocking voussoir systems (e.g., the Abeille system), groups of blocks must be placed in a specific order to create a reciprocal support system.
- In corbelling, the placement of the counterweight (either external infill or bricks) needs to be specifically sequenced to provide adequate counteracting force.

Equipment technology refers to where self-support is a function a global-level mechanical advantage or specific equipment used to provide a counter-balancing force.

- In a cable system construction, a system of cables, pulleys, and weights are hung over a partially completed structural feature to provide a prestressing force to counteract overturning.
- In rib network construction, a system of light props or scaffolding is used to provide bearing support to the ribs before they are completed and become self-supporting.

3.3. Relative classification of methods

The categorization approach discussed in Sections 3.1 and 3.2, and summarized in Table 1, are qualitative due to the challenges involved in comparing such diverse construction methods. A method rarely conforms neatly to a binary classification as either local/global or internal/external; instead, it typically occupies a position along a continuum between these poles. Furthermore, certain methods may exhibit complexity, incorporating multiple support mechanics or design parameters that span various points on the spectrum. However, for the sake of simplicity in comparison and discussion within this section, we have chosen to categorize the methods based primarily on the most prominent structural characteristic. For instance, while the corbelling and interlocking voussoir methods rely on both assembly hierarchy (global) and tessellation geometry (local), we have emphasized the former in corbelling and the latter in interlocking voussoirs as the primary design parameter. Thus, the methods are categorized according to this primary parameter only. The outcomes of this classification process are not intended as definitive quantitative statements regarding these methods, but rather as a means to facilitate a qualitative comparative evaluation and discussion on the adaptability of these methods to robotic assembly.

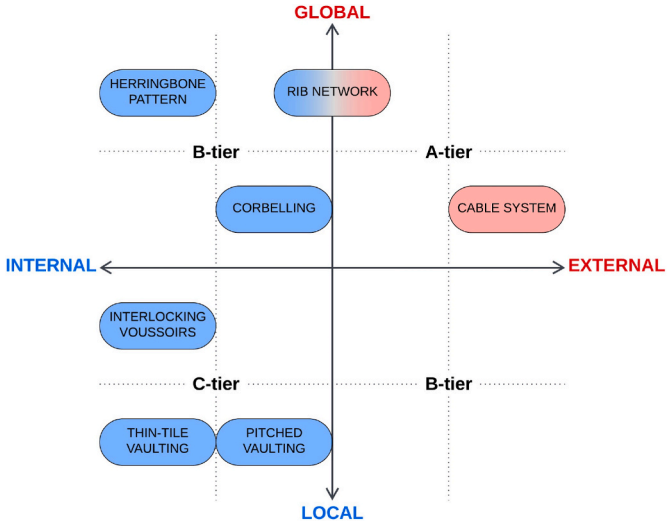

Fig. 9. The construction methods are depicted in a four-quadrant arrangement, categorized according to their primary support mechanism (i.e., internal/external) and primary design parameter (i.e., local/global). These quadrants correspond to tiers indicating the methods' adaptability to cooperative robotic assembly.

In Fig. 9, we present the seven construction methods arranged in a four-quadrant plot, a representation based on considering the two structural criteria as independent binary variables. The x-axis represents the self-supporting structural mechanic (internal/external), while the y-axis represents the primary design parameters (local/global). Recognizing that the methods are more accurately represented on a continuous spectrum, we have further subdivided each quadrant. This allows for a relative arrangement of the methods based on their comparison to similar methods. Here are some justifications for the relative arrangements shown.

- Corbelling is considered more external than the herringbone pattern since there are applications where some degree of external counterweight is utilized.
- Interlocking voussoir construction is considered more global than thin-tile and pitched vaulting as it relies on assembly hierarchy in the sequencing of reciprocal systems.
- Pitched vaulting is considered more external than thin-tile vaulting since it requires some form of backing support to start the construction, which later loses relevance as the construction progresses and the mortar sets.
- The rib network is considered more global than the cable system since the rib network operates on the scale of the full structure, while the cable system is used to target specific regions of a construction.
- The rib network and herringbone pattern are considered more global than corbelling since corbelling relies partly on tessellation geometry, where the seams and sizes of the stones are important parameters.

3.4. Adaptability of methods to cooperative robotic assembly

Local design parameters and internal structural mechanics pose challenges for integration into robotic assembly processes. Given that robotic agents inherently function as external entities in fabrication, their ability to influence factors like friction and interlocking of individual bricks, as well as local design parameters such as material properties and tessellation geometry, is inherently limited. Methods relying heavily on parameters such as the friction of the bonding mortar or specific geometric properties of individual bricks for scaffold-free stability are deemed less suitable specifically for cooperative robotic assembly due to the inability of the robots to work together to effectively control these parameters.

We consider construction methods to be suitable for cooperative robotic adaptability primarily when they require external structural action and rely on executing a cooperative and coordinated series of actions during assembly to achieve stability. Since robots operate as independent external agents in fabrication, methods that minimize scaffolding requirements through external actions can have these external actions performed by robots working together (i.e., several robots can be sequenced to provide support to a structure while simultaneously building the structure). Moreover, global design parameters such as assembly hierarchy are particularly relevant to systems with multiple active robotic agents. For example, planning the use of multiple robots involves sequencing their actions, which is reminiscent to the sequence planning required for masonry methods reliant on assembly hierarchy. Thus, a team of cooperating robots, either working autonomously or in tandem with humans, could be adapted to execute the required coordinated assembly steps required by the method to

accomplish the self-supporting function. Thus, design parameters of assembly hierarchy and equipment technology are readily adaptable to fabrication setups with robots that operate in a flexible and distributed manner on the job site.

Based on this rationale, the least suitable methods for robotic assembly, classified as C-tier, are found in the bottom left quadrant (internal-local) of Fig. 9. These methods rely on both local design parameters and internal structural mechanics for self-support, which as stated are not possible to adapt to a robotic assembly system.

The B-tier methods occupy the top left and bottom right quadrants of Fig. 9. These methods hold potential for robotic assembly. In the top left quadrant (internal-global), the methods depend on internal structural support mechanics, which as explained are challenging to adapt to a robotic assembly system. However, these methods also also rely on assembly hierarchy as a global design parameter for self-support, which is an application that is suitable to a multi robotic system. For example, in the herringbone method, multiple robots could provide support to the horizontal arches while simultaneously adding new bricks to this substructure. Similarly, in corbelling construction, the robots could be sequenced to place the bricks in the correct order and could be planned to act as a temporary counterweight support at critical locations in this sequence.

The bottom right quadrant (external-local) of Fig. 9 presents a paradox, as there are currently no identified methods that rely on both an external structural support mechanic and a primary design parameter operating at the local level of the structure.

The A-tier methods, situated in or touching the top right quadrant (external-global) of Fig. 9, are considered the most adaptable to robotic assembly. The rib network and cable system methods both rely, to some extent, on external support mechanics such as light scaffolding or hanging counterweights, which could be replaced by a robot acting as an external support. Additionally, these methods derive their falsework-minimizing capabilities from global design parameters, which as stated are readily applicable to a setup with multiple robots.

In summary, the seven historic centering-free strategies can be classified into the following three tiers based on their suitability for robotic construction.

A-tier: rib network, cable system
B-tier: herringbone pattern, corbelling
C-tier: pitched vaulting, thin-tile vaulting, interlocking voussoirs

3.5. Selecting the rib network method for further study

The classification exercise leads to the conclusion that both the rib network and cable system methods are the most suitable for adaptation to robotic assembly. However, the rib network method is specifically chosen for further investigation in subsequent computational studies. This choice is based on its potential for broader application, especially in constructing complex vaulted structures, as it offers scalability by allowing modifications to the number and orientation of planar arches in the network without significantly increasing robotic construction complexity (scaling linearly with the number of arches) (Bruun et al., 2021). Another motivation for further study is that the rib network method already has demonstrated examples of its robotic implementation (Parascho et al., 2020; Wu and Kilian, 2018).

On the other hand, the cable system approach exhibits a more specialized nature, being applicable solely to specific masonry geometries as noted in previous research (Fitchen, 1981). Although a robotic setup is suitable to the cable system method by allowing a robot to directly apply pre-stress to localized areas of the structure (eliminating the need for external counterweights), fulfilling this requirement becomes progressively challenging as the size and complexity of the structure increase. For example, the number of pre-stress points grows super-linearly with increasing geometric complexity (Deuss et al., 2014). Thus, the cable system is not considered as scalable as the rib network method when working with a fixed team of cooperating robots.

Fig. 10. The completed LightVault.

4. Computational case studies

To assess the feasibility of adapting the rib network method for robotic assembly, a more in-depth investigation is required, focusing on two critical aspects.

1. Identifying the optimal robotic construction setup for building individual planar arches, as detailed in Section 4.1, with the results discussed in Section 5.1.
2. Establishing the correct sequence for constructing individual arches within the overarching network, as detailed in Section 4.2, with the results discussed in Section 5.2.

4.1. Parametric computational study of planar arch assembly using two cooperating robots

In Section 4.1, the setup for the first computational study is outlined, which evaluates the feasibility, both from geometric and structural perspectives, of assembling individual planar arches in a scaffold-free manner when using a robotic setup. Such a study is necessary as these arches are considered the meso-scale building blocks for the rib network, which can itself be envisioned as an interconnected arrangement of planar arches intended to support the vaulted surface. The goal is to determine the geometric and structural limits of fabrication with two cooperating robotic arms and based on these results determine what the optimal setup would be to use in future work.

4.1.1. The LightVault project as inspiration

This study builds on the cooperative robotic construction methodology first developed in the LightVault project, where a 338-brick doubly-curved masonry vault spanning a plan area of 2670 × 4350mm was constructed using two cooperating robotic arms in such a way that external falsework was not required (Fig. 10). Both a medium-payload robotic setup on a linear track (Parascho et al., 2020) and high-payload fixed robotic setup (Han et al., 2020; Parascho et al., 2021) were explored in previous work. Aside from this published research, additional details of the physical experimentation can be seen in a video documenting the robotic construction process for several prototype structures constructed during the project (CREATE Laboratory Princeton, 2020).

The first construction phase for the vault, which is specifically relevant to this computational study, required constructing a central planar arch that then functioned as the structural backbone for the remaining structure. Notably, it was in the LightVault project first theorized and successfully demonstrated that a planar masonry arch could be constructed without any falsework when using a minimum of two cooperating robotic arms (Parascho et al., 2020). This was accomplished by

Table 2
Parametric study variables and values.

Variable	Values
Arch Span (s)	2m, 3m, 4m, 5m, 6m, 7m
Rise-to-Span (r/s)	0.125, 0.25, 0.375, 0.5, 0.625, 0.75, 0.875, 1.0
Angle (α)	0°, 7.5°, 15°, 22.5°
Robotic Setup	IRB 5710-70/2.70 - On 3.9m Linear Track IRB 6700-235/2.65 - Fixed

Table 3
Number of bricks, total mass, and crown height for all planar arches.

		Arch Span (m)					
		2	3	4	5	6	7
Rise-to-Span	0.125	28	42	56	69	83	97
		76 kg	114 kg	152 kg	187 kg	225 kg	263 kg
		0.25m	0.38m	0.50m	0.62m	0.75m	0.88m
	0.250	31	46	61	77	92	107
		84 kg	125 kg	165 kg	209 kg	249 kg	290 kg
		0.50m	0.75m	1.00m	1.25m	1.50m	1.75m
	0.375	35	52	70	87	105	122
		95 kg	141 kg	190 kg	236 kg	284 kg	331 kg
		0.75m	1.12m	1.50m	1.88m	2.25m	2.62m
	0.500	40	60	80	100	120	139
		108 kg	163 kg	217 kg	271 kg	325 kg	377 kg
		1.00m	1.50m	2.00m	2.50m	3.00m	3.50m
	0.625	45	68	91	113	136	158
		122 kg	184 kg	247 kg	306 kg	368 kg	428 kg
		1.25m	1.88m	2.50m	3.12m	3.75m	4.38m
	0.750	51	77	102	128	153	179
		138 kg	209 kg	276 kg	347 kg	415 kg	485 kg
		1.50m	2.25m	3.00m	3.75m	4.50m	5.25m
	0.875	57	86	114	143	171	200
		154 kg	233 kg	309 kg	387 kg	463 kg	542 kg
		1.75m	2.62m	3.50m	4.38m	5.25m	6.12m
	1.000	63	95	126	158	190	221
		171 kg	257 kg	341 kg	428 kg	515 kg	599 kg
		2.00m	3.00m	4.00m	5.00m	6.00m	7.00m

progressively building the arch from one end, with the two robotic arms working together resulting a cooperative "leapfrogging" sequence, alternating one robot providing temporary support for the unfinished arch while the other placing the next brick (Parascho et al., 2020). Bonding epoxy or mortar is manually placed on each brick before robotic insertion into the structure. This construction approach was then conceptually extended, in the context of studying how the LightVault's planar arch could be constructed more efficiently, by adding a third robot to the cooperative fabrication setup (Bruun et al., 2021). Furthermore, cooperatively sequencing multiple robots to act as either passive agents during construction (i.e., supporting the structure) while take turns as active agents (i.e., placing and/or removing components) has been validated and demonstrated as a viable technique for a wide range of structural systems and applications (Bruun et al., 2020, 2022a, 2022b, 2024b).

The computational studies in this paper are based on the "leapfrogging" sequence methodology demonstrated in the LightVault, but they go further by expanding the exploration space with respect to geometric and robotic parameters. The LightVault project featured a single vault geometry with a central planar arch with a span/height ratio of 2.08/1.93 m, constructed using two medium-payload robotic arms (Bruun et al., 2021). Unlike the singular arch geometry in the LightVault project, our present studies encompass a much broader range of arch geometries. Additionally, we introduce a new parameter by investigating how the construction process is influenced when varying the physical robotic setup from mobile to fixed. Our principal objective with this extensive parametric investigation is to delineate the critical geometric constraints, structural limitations, and the associated trade-offs when employing two cooperating robots in different configurations for scaffold-free construction.

4.1.2. Formulating the parametric study

The computational study explores a range of planar catenary arch geometries, which are defined with the following key variables: arch span, rise-to-span ratio, and inclination angle. Our aim is to conduct a comprehensive exploration, exhaustively studying all combinations of these variables as shown in Table 2. Although certain combinations of these variables may yield arches that exceed practical limits for masonry structures (e.g., a 2-m height with a rise-to-span ratio of 0.125 results in a very small flat arch) they are nevertheless included in this computational study for the sake of comprehensiveness and to better delineated the physical boundaries of the design space (see Table 3).

The top half of Fig. 11 illustrates the influence of varying each of these variables on the resulting arch geometry. While rib networks are typically only composed of arches with an inclination of 0°, inclined arches are possible and are also featured in other methods such as pitched vaulting, thus it was considered relevant to assess the impact of this variable.

Each brick weighs approximately 2.71 kg, assuming a standard brick with dimensions 225x112.5 × 75 mm made from a material with a specific weight of 14 kN/m^3. Given the values of span and rise-to-span ratio defined in Table 2, the resulting number of bricks (n), total masses, and the crown heights for the forty-eight different arch geometries are shown in Table 3. These values would be the same across all corresponding arches at all inclination angles (e.g., an arch at 0° will be the same at 15°, just rotated about an axis defined by its base points). The planar arch geometries generated in this parametric study are provided as a supplementary file accompanying the research paper.

In addition to varying arch geometry, we also explore the diversity in robotic assembly setups employed during arch construction. All setups adhere to a cooperative configuration involving two robotic arms, a minimum requirement for effective collaboration that has demonstrated the capability to construct planar arches without the need for scaffolding. The variation in robot size serves to investigate the fundamental trade-off inherent in robotic assembly processes, specifically the balance between payload capacity and maneuverability/reach. Smaller and more agile systems possess greater maneuverability and reach, but compromise on their ability to support substantial payloads since they are not anchored to resist overturning. Our exploration encompasses three overarching categories of 6-axis robotic arm setups.

- low-payload/high-maneuverability: Robotic arms on a wheeled chassis, providing unrestricted movement at the cost of low payload capacity (~5–20 kg).
- medium-payload/medium-maneuverability: Robots with constrained movement along a linear track, offering a medium payload capacity (~20–80 kg) (ABB Ltd., 2023).
- high-payload/low-maneuverability: Robots firmly anchored to the ground, achieving the highest payload capacity (~80–500 kg) (ABB Ltd., 2023).

Only the medium-payload and high-payload setups are studied in further detail as the low-payload setup is not viable for structural scale construction when the robots are required to provide a support function (i.e., maximum payload is quickly exceeded). The arrangement of the two selected setups chosen for further study are shown at bottom of Fig. 11.

4.1.3. Evaluation criteria for the parametric study

To systematically evaluate the parametrically generated arches, two essential construction feasibility metrics were assessed: (1) fabrication score, and (2) robotic loading. The parametric computational workflow, outlined in this section, was implemented in a Rhino/Grasshopper script (Rutten, 2007). A high-level schematic depiction of this computational process can be found in Appendix B.

The first construction feasibility metric, known as the fabrication score, served as a proxy for gauging the ease of fabricating the arch using

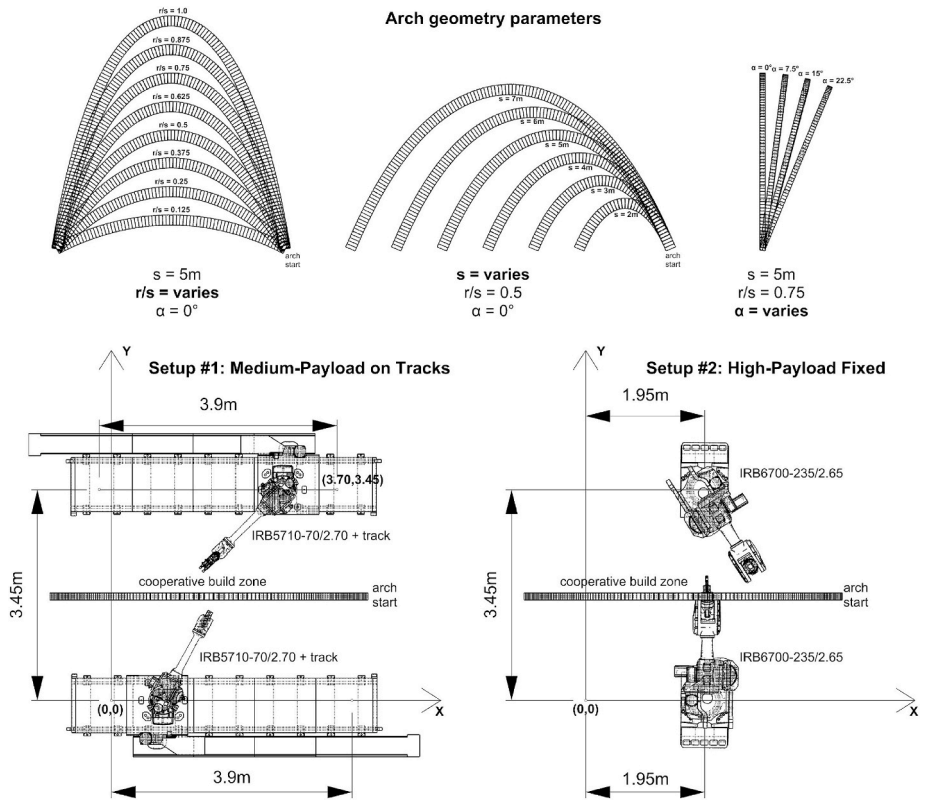

Fig. 11. Parametric definition of the planar arch geometries (top) and the layout of the robotic assembly setups (bottom) investigated in the computational study.

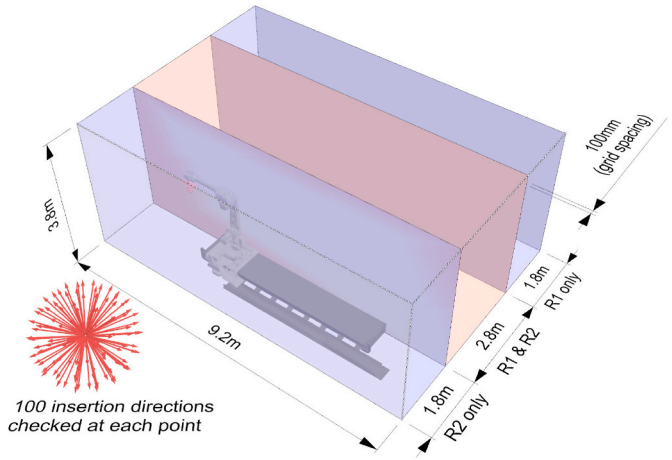

Fig. 12. Volume encompassing the cooperative robotic setup discretized into a 100 mm grid and mapped with inverse kinematic checks. The cooperative zone (red) is defined as the union of the volumes checked for each individual robot (R1 or R2).

the designated robotic setup. To perform this evaluation, the entire construction volume, measuring 9.2x6.4 × 3.8 m, was first discretized into a grid of points spaced at 100 mm intervals, resulting in a total of 235,755 points. Each robot was allocated a distinct subsection of this volume, defining its maximum reach, resulting in 170,469 unique points for each robot. The "cooperative zone," where both robots could potentially collaborate on fabrication tasks, was defined as the overlapping volume of 9.2x2.8 × 3.8 m (approx. 44% of total volume), encompassing 105,183 points, formed as a union of their individual volumes (see Fig. 12).

Next, at each point within the construction volume designated for a robot, a series of inverse kinematic checks were performed, simulating its reach from 100 different insertion directions. For each direction where the robot could successfully reach, indicated by the existence of a valid inverse kinematic solution, the reachability value for that specific point was incremented by one. Consequently, in a cooperative setup involving two robots, the maximum theoretical reachability value for a point within the cooperative zone would be 200 (signifying that each robot could reach it from all 100 directions), while it would be 100 in a non-cooperative zone. However, in practice, achieving perfect reachability was rare due to certain orientations being challenging for a specific robot (e.g., in the case of a robot having to stretch out fully and simultaneously reach back 180°). To compile this comprehensive reachability dataset for both setups, ~68 million unique inverse kinematic checks were performed (i.e., 2 setups × 2 robots per setup x 170,469 points per robot x 100 inverse kinematic checks per point), which took ~40 days of computation (wall time, system agnostic) to complete when setting a 0.05 s timeout per inverse kinematic check. The generated reachability map datasets, for both robotic setups, are included as supplementary files with the research paper. The dataset for the fixed setup is filtered to remove points at either end of the search volume that are definitely not reachable.

Once the construction volume had been mapped using this method, it became possible to calculate a fabrication score for any structure intended to be constructed with that specific robotic configuration. This process involved superimposing the structure, in this instance, a masonry arch, onto the discretized fabrication volume. Subsequently, the reachability values associated with the point nearest to the centroid of each brick were summed and then divided by the total number of bricks to generate the fabrication score. In addition to this value, an assessment was also made to determine what percentage of the arch structure fell within the cooperative fabrication zone, where both robots could access it from at least one direction. Arch structures with a cooperative reach score between 98 and 100% were deemed suitable for cooperative construction, assuming that while a few bricks at the start of the arches

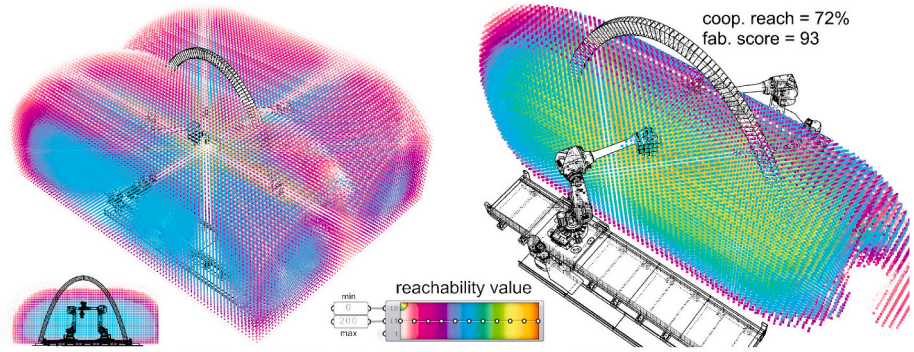

(a) Medium-payload robot linear track setup, showing the full (left) and cooperative (right) reachability maps

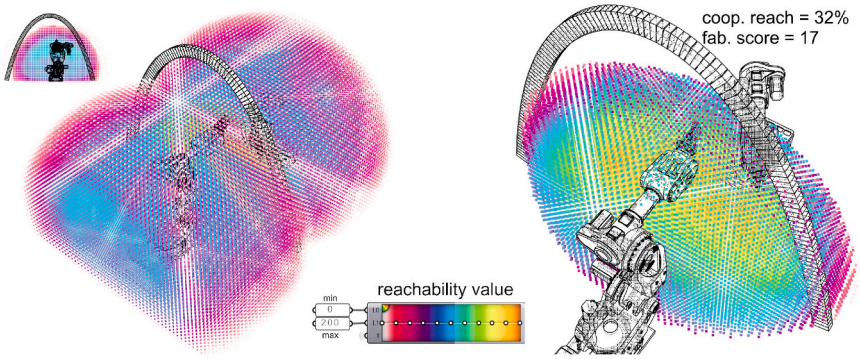

(b) High-payload fixed robot setup, showing the full (left) and cooperative (right) reachability maps

Fig. 13. Mapping the construction volume through discrete reachability checks for both cooperative robotic setups. This dataset is used to calculate the fabrication score for a structure. Showing an example arch ($\alpha = 0°$, s = 5 m, r/s = 0.75) and its resulting fabrication score with both setups.

might be difficult to reach robotically these could easily be placed by hand without impacting the rest of the robotic construction process. Those arches falling outside this range would present significant challenges due to needing to robots to execute the "leapfrogging" sequence effectively. The mapping of the construction volume for both setups is displayed in Fig. 13, featuring an arch (generated with parameters: $\alpha = 0°$, s = 5 m, r/s = 0.75) and its fabrication and cooperative reach scores depicted when fabricated with either setup.

The second construction feasibility metric, known as the robotic loading, was designed to evaluate the maximum support forces that the robotic arms were expected to encounter throughout the entire cooperative fabrication process. The primary objective of this metric was to determine constructability from a loading perspective, with a focus on assessing whether the robots' payload capacities were exceeded during construction. If such an exceedance did occur, the goal was to identify at what percentage of the arch could be constructed before the limits were reached. To conduct this assessment, a linear elastic finite element analysis (FEA) was performed using Karamba3D (Preisinger and Heimrath, 2014). In this analysis, the bricks were modeled as beam elements with calibrated joints, and the robotic support on the partially completed arch was represented as a pin support. For a more comprehensive explanation of this methodology and further examples of its implementation refer to (Bruun et al., 2021).

4.2. Discrete element computational study of rib network assembly using cooperating robots

In this section, the setup of the second computational study is outlined. This study builds on the results of the planar arch computational study but increases the complexity by examining how multiple cooperative robots should be sequenced for the construction of rib networks comprising three or more arches, as first proposed in (Bruun et al., 2021). While this specific simulation involves three robots collaborating on three arches as a fundamental building block for ribbed shell

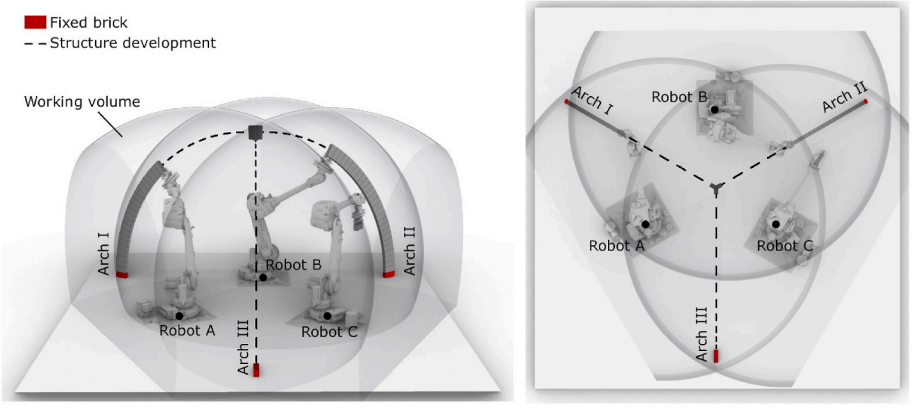

Fig. 14. Schematic layout of the three cooperating fixed high-payload robots in the computational study on the assembly of a rib network.

Table 4
Results from the simulated cooperative robotic construction of planar arches with 0° inclination. Showing the percentage of the arch that is reachable cooperatively (C) and what the resulting fabrication score (fab) is for the arch, and the maximum payloads supported by the robots during constructions (max) and snapshots of the support payloads at 50%, 75% completion of the arch.

(a) medium-payload robots on tracks: robotic reachability data for complete arch

Rise-to-Span \ Arch Span [m]	2	3	4	5	6	7
0.125	C:100% fab:133	C:100% fab:149	C:100% fab:161	C:100% fab:165	C:100% fab:164	C:93% fab:149
0.250	C:100% fab:153	C:100% fab:167	C:100% fab:171	C:100% fab:171	C:100% fab:166	C:93% fab:143
0.375	C:100% fab:162	C:100% fab:170	C:100% fab:172	C:100% fab:168	C:100% fab:153	C:93% fab:105
0.500	C:100% fab:165	C:100% fab:171	C:100% fab:168	C:100% fab:149	C:100% fab:112	C:65% fab:57
0.625	C:100% fab:167	C:100% fab:169	C:100% fab:151	C:100% fab:114	C:69% fab:81	C:32% fab:39
0.750	C:100% fab:168	C:100% fab:162	C:100% fab:125	C:72% fab:93	C:57% fab:64	C:25% fab:32
0.875	C:100% fab:167	C:100% fab:147	C:81% fab:104	C:62% fab:80	C:49% fab:54	C:22% fab:28
1.000	C:100% fab:166	C:100% fab:128	C:70% fab:91	C:54% fab:71	C:43% fab:47	C:19% fab:25

(b) high-payload fixed robots: robotic reachability data for complete arch

Rise-to-Span \ Arch Span [m]	2	3	4	5	6	7
0.125	C:100% fab:99	C:100% fab:114	C:100% fab:118	C:93% fab:106	C:77% fab:90	C:66% fab:78
0.250	C:100% fab:110	C:100% fab:123	C:100% fab:126	C:91% fab:114	C:75% fab:93	C:62% fab:76
0.375	C:100% fab:114	C:100% fab:126	C:100% fab:134	C:90% fab:106	C:69% fab:72	C:52% fab:52
0.500	C:100% fab:116	C:100% fab:126	C:100% fab:127	C:89% fab:75	C:49% fab:37	C:36% fab:28
0.625	C:100% fab:115	C:100% fab:121	C:100% fab:104	C:73% fab:34	C:32% fab:21	C:27% fab:16
0.750	C:100% fab:113	C:100% fab:110	C:100% fab:73	C:32% fab:17	C:24% fab:13	C:20% fab:11
0.875	C:100% fab:108	C:100% fab:94	C:70% fab:52	C:24% fab:12	C:20% fab:10	C:17% fab:8
1.000	C:100% fab:102	C:85% fab:75	C:60% fab:42	C:20% fab:9	C:16% fab:7	C:14% fab:6

(c) medium-payload robots on tracks: robotic support payloads (kg) during construction

Rise-to-Span \ Arch Span [m]	2	3	4	5	6	7
0.125	max:59 75%:34 50%:15	max:103 75%:71 50%:27	max:148 75%:110 50%:48	max:189 75%:150 50%:78	max:233 75%:190 50%:112	max:275 75%:233 50%:149
0.250	max:53 75%:35 50%:16	max:82 75%:59 50%:29	max:111 75%:82 50%:50	max:141 75%:106 50%:71	max:169 75%:127 50%:91	max:197 75%:149 50%:113
0.375	max:54 75%:33 50%:16	max:81 75%:52 50%:27	max:109 75%:72 50%:42	max:136 75%:89 50%:58	max:164 75%:109 50%:73	max:191 75%:127 50%:87
0.500	max:58 75%:34 50%:14	max:88 75%:52 50%:25	max:117 75%:70 50%:37	max:146 75%:88 50%:49	max:176 75%:105 50%:62	max:204 75%:121 50%:73
0.625	max:64 75%:36 50%:14	max:96 75%:54 50%:23	max:129 75%:72 50%:34	max:160 75%:91 50%:44	max:193 75%:109 50%:54	max:224 75%:127 50%:64
0.750	max:71 75%:38 50%:14	max:107 75%:59 50%:22	max:142 75%:78 50%:30	max:179 75%:97 50%:40	max:214 75%:116 50%:49	max:250 75%:135 50%:58
0.875	max:79 75%:42 50%:13	max:119 75%:64 50%:20	max:158 75%:85 50%:28	max:198 75%:104 50%:37	max:236 75%:124 50%:45	max:276 75%:146 50%:53
1.000	max:86 75%:44 50%:13	max:130 75%:67 50%:20	max:173 75%:92 50%:26	max:217 75%:114 50%:34	max:261 75%:137 50%:42	max:304 75%:159 50%:50

(d) high-payload fixed robots: robotic support payloads (kg) during construction

Rise-to-Span \ Arch Span [m]	2	3	4	5	6	7
0.125	max:59 75%:34 50%:15	max:103 75%:71 50%:27	max:148 75%:110 50%:48	max:189 75%:150 50%:78	max:233 75%:190 50%:112	max:275 75%:233 50%:149
0.250	max:53 75%:35 50%:16	max:82 75%:59 50%:29	max:111 75%:82 50%:50	max:141 75%:106 50%:71	max:169 75%:127 50%:91	max:197 75%:149 50%:113
0.375	max:54 75%:33 50%:16	max:81 75%:52 50%:27	max:109 75%:72 50%:42	max:136 75%:89 50%:58	max:164 75%:109 50%:73	max:191 75%:127 50%:87
0.500	max:58 75%:34 50%:14	max:88 75%:52 50%:25	max:117 75%:70 50%:37	max:146 75%:88 50%:49	max:176 75%:105 50%:62	max:204 75%:121 50%:73
0.625	max:64 75%:36 50%:14	max:96 75%:54 50%:23	max:129 75%:72 50%:34	max:160 75%:91 50%:44	max:193 75%:109 50%:54	max:224 75%:127 50%:64
0.750	max:71 75%:38 50%:14	max:107 75%:59 50%:22	max:142 75%:78 50%:30	max:179 75%:97 50%:40	max:214 75%:116 50%:49	max:250 75%:135 50%:58
0.875	max:79 75%:42 50%:13	max:119 75%:64 50%:20	max:158 75%:85 50%:28	max:198 75%:104 50%:37	max:236 75%:124 50%:45	max:276 75%:146 50%:53
1.000	max:86 75%:44 50%:13	max:130 75%:67 50%:20	max:173 75%:92 50%:26	max:217 75%:114 50%:34	max:261 75%:137 50%:42	max:304 75%:159 50%:50

structures, the principles explored in this study can be extended to more complex scenarios involving additional arches. The goal is to provide insights into the optimal construction order, robotic coordination and sequencing, and to establish a comprehensive foundation for the understanding of the challenges and opportunities presented by cooperative robotic in rib network construction.

4.2.1. Formulating the computational study

The computational study involved simulating the construction of three planar arches, denoted as Arch I, Arch II, and Arch III, which collectively constitute a basic rib network. This network is constructed collaboratively using three high-payload fixed robots. These robots were selected based on the results of the planar arch parametric study Section 5.1, which identified them as the most suitable choice for centering-free assembly of masonry arches. The three robotic arms, designated as A, B, and C, are strategically positioned in a triangular configuration. This arrangement maximizes the cooperative fabrication zone between them and enables each robot to access two separate arches, as depicted in Fig. 14.

Within the computational study, we formulate and investigate two distinct yet viable cooperative assembly sequences. Our aim is to determine which of these sequences is more optimal.

1. Sequential Assembly (SeA): In this sequence, Arch I is built sequentially by Robots A and B. Once Arch I is complete, Robot A continues to support Arch I, while Robot B collaborates with Robot C to construct Arch II. Next, Robot B supports Arch I & II while Robots A and C collaborate to build Arch III.
2. Simultaneous Assembly (SiA): In this sequence, all three robots are working concurrently to construct both Arch I and Arch II. Once

these two arches are complete, Robot B supports them while Robot A and C then collaborate to build Arch III.

4.2.2. Evaluation criteria for the computational study

The assembly process was simulated using Discrete Element Analyses (DEM) with the commercially available DEM software, 3DEC (Itasca Consulting Group Inc, 2016). In this numerical approach, masonry structures were represented as an ensemble of interacting blocks, with the bricks being treated as rigid bodies capable of sliding, rotating, or colliding. The connections between these bricks were modeled using interfaces governed by a Mohr-Coulomb model (Simon and Bagi, 2016), with parameters tailored to the mortar characteristics. Specifically, a cohesion value of 10 kPa was selected, with a tensile stress cut-off at 10 kPa. Joint stiffness and shear stiffness were defined as $jK_n = 100 \times 10^{10}$ kN/m^3 and $jK_s = 10 \times 10^9$ kN/m^3, respectively, while the friction angle was set at 25° based on (Simon and Bagi, 2016). This computational approach follows the methodology and uses the same parameter values as defined in previous work (Paris et al., 2021).

The displacements of the arches during all three phases (Phase I, Phase II, and Phase III) were evaluated in both assembly sequences. Furthermore, the time needed to complete the entire rib network construction was estimated based on the number of steps each sequence required. These parameters served as vital criteria for evaluating and selecting the preferred robotic assembly sequence.

5. Results and discussion of computational case studies

In the following section the results of the computational case studies described in Section 4 are presented, starting with the planar arch study in Section 5.1 and followed by the rib network assembly study in Section 5.2.

5.1. Planar arch parametric study

The results of the planar arch parametric study for a 0° inclination scenario are presented in Table 4. The reachability and support load data for the medium-payload robot are shown in Tables 4a and 4c, while the reachability and support load data for the high-payload fixed robot configuration are shown in Tables 4b and 4d. The reachability and support load data for arch inclinations other than 0° are consolidated in Appendix A, specifically in Table A1 and Table A2. Consistent trends are evident across all arch inclinations; thus, this section will primarily focus discussions on the 0° inclination case.

Tables 4a and 4b provide data on the reachability metric and showcase the percentage of each arch falling within the cooperative zone and present the overall fabrication score for the entire arch. The fabrication score represents the average reachability values for all the bricks forming the arch. Arch designs with a cooperative percentage ranging from 98% and above are deemed suitable for cooperative fabrication. Those with cooperative percentages between 80 and 98% are highlighted in yellow, indicating that they are close to being feasible with the specific robotic configuration. Conversely, arch designs falling below the 80% mark are marked in red, indicating their infeasibility with the given setup. As expected, the robotic setup equipped with linear tracks outperforms the fixed robotic setup in terms of reachability. In the 2–3 m span range, all arches comfortably fall within the cooperative zone of this setup. Additionally, most arches with rise-to-span ratios up to 0.5 are also within the realm of feasibility. Out of the forty-eight tested arches, the highest fabrication score achieved is 172, notably occurring for the arch with a 4-m span and a rise-to-span ratio of 0.75.

Conversely, the fixed robotic setup exhibits limited reach, evident from the larger proportion of arches falling into the unreachable zone. Specifically, only arches with spans below 5 m fall within the cooperative zone of the setup. Even within this subset of smaller spans, arches with higher rise-to-span ratios exceeding 0.75 are typically not constructible. Consistently across the entire dataset, fabrication scores for corresponding arches are notably lower for the fixed setup. On average, these scores are approximately 50 points lower compared to the medium-payload setup, with average scores of 76 and 127, respectively. An interesting observation is that the highest fabrication score, totaling 134, observed for the high-payload setup also corresponds to the 4-m span arch with a rise-to-span ratio of 0.375.

The discrete fabrication scores from Tables 4a and 4b are linearly interpolated and then depicted as contour plots in Fig. 15, offering a visual representation of the relative differences in fabrication performance between the two setups. A perfect reach score for a single robot is 100, making this contour line a rough indicator of where cooperative action commences, albeit not a definitive dividing line, as it is possible for two robots to reach all bricks within an arch but only in few ways, resulting in a combined score below 100. The region above 100 for the medium-payload setup is significantly larger than for the high-payload setup. Additionally, Fig. 15 illustrates that the medium-payload setup exhibits a flatter slope around the maximum fabrications score location, indicating that fabrication performance is not sensitive to varying the values of the parameters in this region. Thus, a large range of different arches are easily fabricated. Conversely, the slope towards the bottom

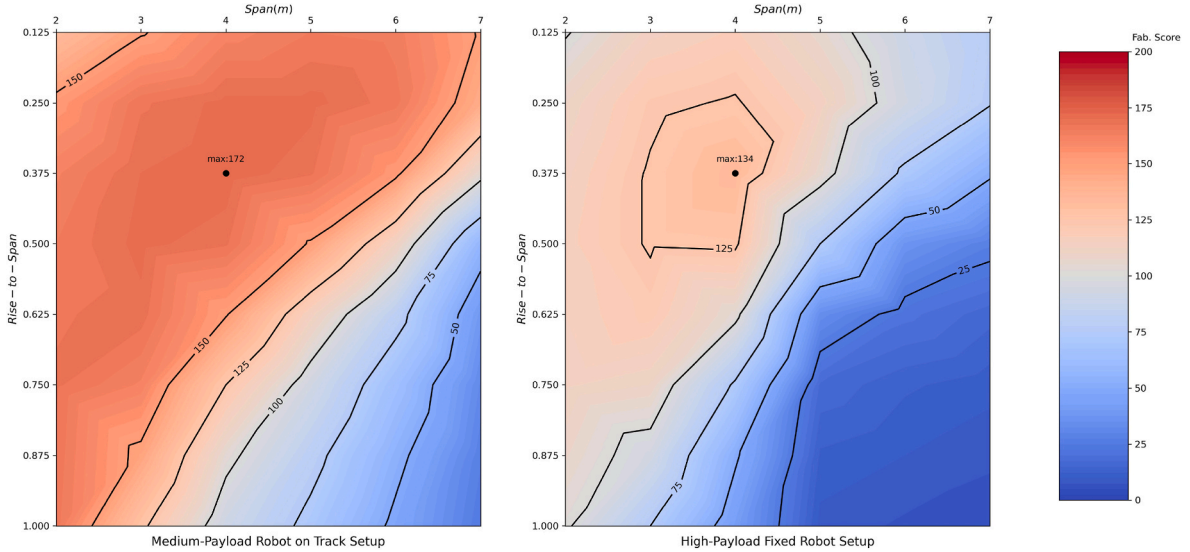

Fig. 15. Contour plots of linearly interpolated fabrication scores from Tables 4a and 4b as a function of span and rise-to-span for arches with 0° inclination.

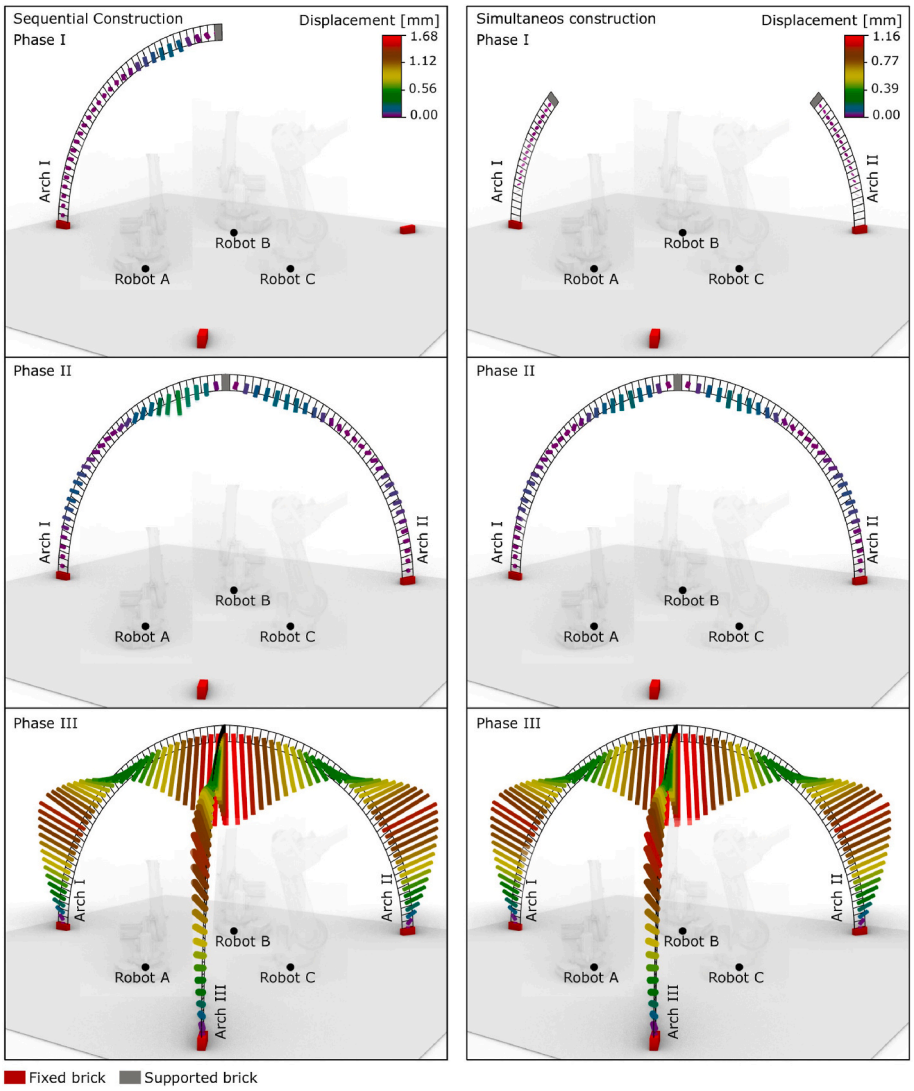

Fig. 16. Simulating the scaffold-free assembly of a rib network with three cooperating fixed high-payload robots showing the displacements results during the phases of the Sequential Construction method (left) and Simultaneous Construction method (right).

right of the plots, corresponding to arches with larger spans and rise-to-span ratios, is notably steeper for the high-payload configuration, signifying that arches swiftly become unbuildable with this setup as they grow, with a substantial region below a score of 25.

In Tables 4c and 4d, data regarding the support loading experienced by the robots during construction using a ”leapfrogging” sequence is presented. If the maximum support load calculated for a robot in a specific setup falls below 70 kg for the medium-payload configuration or 235 kg for the high-payload configuration, the arch is deemed suitable for scaffold-free construction. Arch designs where these payload limits are exceeded, ranging from 75 to 100% of the total arch assembly, are highlighted in yellow, signifying their proximity to feasibility with the specific robotic configuration. Conversely, arch designs resulting in the robots reaching their payload limits before completing 75% of the arch are marked in red, indicating their infeasibility with the provided setup.

Upon examination of the support load data, a distinct reversal in performance trends emerges between the two setups, with the high-payload fixed configuration demonstrating a significant advantage over the medium-payload setup. The former can provide support for all arches, except for a few at the study’s outer boundaries, which encounter challenges during the 75–100% range of construction. Conversely, the medium payload setup proves incapable of supporting any arches with spans surpassing 4 m, and many of the remaining arches experience difficulties in the 75–100% range of construction, with only 5 exceptions falling within the payload capacity.

In summary, similar performance trends are observed in planar arch construction for both medium-payload robots on tracks and high-payload fixed robots. These trends are a reduction in fabrication score and an increase in support payload requirements as arch spans and rise-to-span ratios increase. While the choice between these robotic systems should always consider project-specific requirements, several over-arching conclusions can be drawn from this computational study. The mobile robots can reach a wider range of designs while the high-payload robots are able to assemble larger structures. For example, the limitations imposed by payload exceedance on scaffold-free construction for the medium-payload mobile setup surpass the reachability restrictions

imposed by the high-payload fixed setup. Consequently, despite its inferior performance in the reachability metric, the high-payload fixed robot configuration emerges as the more suitable choice for the scaffold-free construction of larger planar arches. Although the medium-payload setup excels in reachability across all arch geometries, the support load performance unequivocally favors the high-payload fixed configuration. It demonstrates a capacity to support all arches, with minor challenges encountered at the study's periphery. In contrast, the medium-payload setup's limitations are stark, while it can cooperatively reach a much larger range of geometries the crucial limitations are that it can only fully support a small range of arches in the 2-m spans with rise-to-span ratios below 0.75.

5.2. Rib network assembly study

Based on the findings from the planar arch parametric study detailed in Section 5.1, it was concluded that constructing a more complex structure of a rib network consisting of three arches would by more suited to using a fixed setup since the mobile setup would be significantly limited by its payload capacity.

Individual arches within the rib network were set to a 3-m span with a rise-to-span ratio of 0.5. These parameters result in an arch geometry that is situated within the region close to the optimal fabrication score for the fixed setup as seen in Fig. 15 while ensuring that the maximum payloads experienced by the fixed robots would remain below their maximum capacities as shown by the load data in Table 4d. Conversely, while the medium-payload robots would also be able to reach this geometry without any issues, the support payloads they would experience would exceed their maximum capacities as shown by the load data in Table 4c.

Both assembly sequences explored yielded structurally viable results, showcasing the effectiveness of both Sequential Assembly (SeA) and Simultaneous Assembly (SiA) approaches. The maximum displacements observed were approximately 1.68 mm for SeA and 1.16 mm for SiA. These small displacements relative to the span indicate that both strategies successfully achieved the goal of constructing stable rib networks comprising three arches.

In the context of Phase II (as illustrated in Fig. 16), SeA exhibited larger and asymmetric displacements during construction compared to SiA, with maximum displacements of 0.32 mm and 0.28 mm, respectively. This variation can be attributed to the different interactions between Arch I and Arch II resulting from the timing of keystone placement. It is worth noting that despite these variations, both sequences resulted in structurally sound constructions.

To estimate the time required for the entire assembly process, we considered several factors. These factors included a brick delivery velocity of 50 mm/s, a setting time of 10 s for each brick, and an additional 20 s for picking and releasing. Consequently, the estimated time to complete the SeA task was approximately 11.43 h, while for SiA, it was 9.25 h, which is a reduction of almost 25%. This time difference highlights the efficiency gains achievable through simultaneous assembly, as it reduced the overall construction time compared to the sequential approach.

In summary, the primary focus of this study was directed toward addressing the challenge of coordinating cooperative robotic sequences for the construction of rib networks without the utilization of external scaffolding or any supporting structure. The conclusions are based on the discrete element structural analysis conducted during the assembly of a network comprising three arches. The findings validate the feasibility of both SeA and SiA construction sequences, while emphasizing the potential advantage of the latter in terms of construction time. The insights from this computational study extend beyond this specific three-arch scenario and can be extrapolated to encompass more intricate structures with more ribs within the realm of ribbed shell construction. As the adoption of robotics within the construction industry continues to grow, these computational studies furnish valuable guidance for the optimization of cooperative construction processes in the context of constructing architecturally innovative structures.

6. Conclusion

The research presented in this paper highlights the potential advantages of evaluating historical construction techniques through the lens of modern robotic fabrication, with the goal of advancing sustainable construction by eliminating the need for centering in masonry vaults. This research also adds to the discussion on how best to combine tradition and innovation in the development of contemporary construction methods by promoting the integration of traditional techniques into emergent digital and automated construction processes.

This paper has contributed to the existing literature on the use of cooperative robotic assembly setups to enhance efficiency in masonry construction, facilitate the assembly of intricate structures, stimulate architectural creativity, and address environmental concerns by minimizing the need for centering. Through a parametric exploration of the design space encompassing masonry arches and rib networks constructed with diverse cooperative robotic setups, we delineate the physical boundaries for spanning masonry structures built with multiple robots. Consequently, the computational studies offer insights for architects and engineers, guiding them in navigating the parameters governing spanning masonry structures designed for robotic assembly. In Section 6.1 we summarize the main findings in this paper and make conclusions about the viable design space with respect to the different cooperative robotic fabrication setups.

6.1. Summary of main findings

This paper provided a comprehensive overview of seven historical construction techniques employed to reduce the necessity for centering in masonry vault construction. These strategies were presented with concise summaries, accompanied by schematic illustrations and real-world examples, rendering them a valuable resource for structural designers, architects, and builders interested in incorporating traditional methods into current design practices.

To evaluate the adaptability of these seven centering-minimizing strategies to robotic fabrication technology, a qualitative classification system was developed based on the self-supporting structural mechanic and primary structural design parameters present in each method. This classification approach was deemed essential to create a unified framework for assessing such a wide range of differing construction strategies. Following the development of this system and the sorting of the methods, the rib network centering-minimizing construction method was identified as the most suitable for adaptation to a cooperative robotic assembly setup.

With the rib network chosen for further investigation, the subsequent objective was to determine to what extent this construction method was better suited to a medium-payload robot on a linear track or a high-payload fixed robot cooperative assembly setup. Two computational case studies were conducted to assess the viability of these distinct setups: (1) the construction of a series of planar arches and (2) the assembly of a rib network without the necessity for centering. Through the case study on planar arch construction, it was discerned that achieving centering-free construction for various arch geometries hinged on the superior support capacity afforded by the high-payload fixed robot configuration. Despite the medium-payload mobile setup consistently exhibiting superior reachability scores across all arch geometries, with a peak score of 174/200 for the 4-m span arch with a rise-to-span ratio of 0.75, this advantage was overshadowed by the frequent surpassing of support payload limits. Consequently, this design space exploration has shown that medium-payload robots are viable only for fabricating arches with spans of 2 m or less, which would result in a structure that is outside the range of comfort for a person to occupy. In contrast, high-payload robots demonstrated the capacity to fabricate arches with

spans of up to 4 m, ensuring structural stability during construction for a more substantial subset of arches that can be used to build structures that fall within more practical architectural scales.

These findings established the high-payload fixed robot setup as the preferred choice for centering-free construction of larger and more complex masonry rib structures as the payload constraint in the medium-payload setup was excessively limiting. These conclusions formed the basis for the development of a discrete element case study centered on the construction of a more complex rib network, employing a cooperative robotic arrangement comprising three fixed high-payload robots. Two distinct assembly sequences for the rib network were explored, demonstrating the feasibility of both sequential and simultaneous construction approaches. Nevertheless, it was observed that the simultaneous construction method resulted in reduced displacements (e.g., 0.32 versus 0.28 mm) and expedited completion of the construction when compared to the sequential construction method (e.g. 9.25 versus 11.43 h).

6.2. Limitations and future work

This research has yielded valuable insights into the practicality of employing cooperative robotic systems in constructing spanning rib networks and planar arches while minimizing centering requirements. While the benefits of reducing material usage are evident in scaffold-free construction, the economic ramifications of substituting human labor with robots on site warrant further investigation. Furthermore, the computational analyses presented in this paper lay the groundwork for future validation through experimental initiatives, utilizing robot teams to assemble larger and more intricate masonry structures than previously attempted, as seen in projects like the LightVault. Additionally, the insights gleaned from the planar arch parametric study highlight the necessity of exploring methods to enhance the payload capacity of mobile robots or facilitate mobility for larger robotic units. Improved payload capacity offers clear advantages for construction projects at the building scale, prompting continued exploration in this area.

It is also important to acknowledge certain limitations that warrant consideration. We recognize that the study is limited to two specific robotic assembly setups and that for better generalization additional configurations should be studied in the future. We also recognize several challenges and shortcomings inherent in our approach, particularly regarding the unforeseeable additional complexities in construction that may not be fully captured through digital simulations alone. For example, there are many aspects (i.e., calibration, temperature changes, human error, end-effector variability etc.) that could jeopardize the accuracy of the assembly process and therefore influence the structural capacities of the vault. Although our previous physical experimentation has demonstrated a significant tolerance for errors in brick placement within robotically assembled masonry structures (Parascho et al., 2021), where such errors can be compensated for by the application of mortar, this acceptable error should be further investigated and quantified. Furthermore, to enhance the practical applicability of the proposed technique in real-world construction scenarios, future research should delve into the transportation and setup process of the robotic teams and how to create an adequately structured environment at the designated construction site. For the rib network construction method specifically, a comprehensive overview of construction methods for spanning the space between ribs would contribute to a more nuanced understanding of the implementation challenges and practical feasibility of this method. Addressing these limitations in future work will not only refine this proposed construction method but also generally pave the way for more robust and applicable advancements in the field of robotic construction at the building scale.

CRediT authorship contribution statement

Edvard P.G. Bruun: Writing – review & editing, Writing – original draft, Visualization, Validation, Software, Project administration, Methodology, Investigation, Conceptualization. **Robin Oval:** Writing – review & editing, Writing – original draft, Methodology, Investigation, Conceptualization. **Wesam Al Asali:** Writing – review & editing, Writing – original draft, Conceptualization. **Orsolya Gáspár:** Writing – review & editing, Visualization. **Vittorio Paris:** Writing – review & editing, Visualization, Validation. **Sigrid Adriaenssens:** Writing – review & editing, Funding acquisition.

Declaration of competing interest

The authors declare that they have no known competing financial interests or personal relationships that could have appeared to influence the work reported in this paper.

Data availability

Data is included as supplementary files

Acknowledgements

We gratefully acknowledge the generous support received from various organizations, including the National Science Foundation (Grant No. 2122271), the Fung Global Fellows Program at Princeton University, the PIIRS ROBELARCH Global Collaborative Research Network, and the Thomas Cholnoky Foundation. 3DEC Software was provided by Itasca C.G. under the Education Partnership Program. This publication was supported by the Princeton University Library Open Access Fund.

Appendix ASupplementary data

Supplementary data to this article can be found online at https://doi.org/10.1016/j.dibe.2024.100516.

Appendix A. Results from the simulated cooperative robotic construction of inclined planar arches

Table A.1
robotic reachability data (left) and robotic support payloads (right) in planar arch construction with two medium-payload robots on tracks

(a) 7.5° arch inclination: robotic reachability data

Rise-to-Span \ Span [m]	2	3	4	5	6	7
0.125	C:100% fab:132	C:100% fab:148	C:100% fab:161	C:100% fab:165	C:100% fab:163	C:93% fab:149
0.250	C:100% fab:154	C:100% fab:166	C:100% fab:170	C:100% fab:171	C:100% fab:165	C:93% fab:143
0.375	C:100% fab:161	C:100% fab:171	C:100% fab:171	C:100% fab:167	C:100% fab:151	C:91% fab:105
0.500	C:100% fab:166	C:100% fab:171	C:100% fab:165	C:100% fab:148	C:85% fab:107	C:47% fab:52
0.625	C:100% fab:167	C:100% fab:168	C:100% fab:150	C:80% fab:111	C:62% fab:78	C:27% fab:37
0.750	C:100% fab:168	C:100% fab:160	C:88% fab:122	C:66% fab:91	C:52% fab:63	C:23% fab:32
0.875	C:100% fab:167	C:100% fab:147	C:72% fab:103	C:56% fab:78	C:44% fab:53	C:20% fab:28
1.000	C:100% fab:164	C:88% fab:125	C:63% fab:90	C:49% fab:69	C:38% fab:46	C:18% fab:25

(b) 7.5° arch inclination: robotic support payloads (kg)

Rise-to-Span \ Span [m]	2	3	4	5	6	7
0.125	max:64 75%:40 50%:16	max:108 75%:80 50%:34	max:151 75%:119 50%:61	max:191 75%:159 50%:96	max:232 75%:198 50%:133	max:274 75%:238 50%:172
0.250	max:54 75%:37 50%:19	max:82 75%:61 50%:34	max:109 75%:82 50%:56	max:139 75%:106 50%:77	max:166 75%:127 50%:97	max:194 75%:148 50%:118
0.375	max:53 75%:34 50%:18	max:80 75%:52 50%:30	max:107 75%:72 50%:46	max:134 75%:88 50%:61	max:161 75%:108 50%:75	max:188 75%:126 50%:89
0.500	max:57 75%:34 50%:16	max:86 75%:52 50%:27	max:115 75%:69 50%:39	max:144 75%:87 50%:51	max:173 75%:104 50%:63	max:200 75%:121 50%:74
0.625	max:62 75%:36 50%:15	max:95 75%:54 50%:25	max:127 75%:72 50%:36	max:157 75%:90 50%:45	max:189 75%:108 50%:55	max:220 75%:127 50%:65
0.750	max:70 75%:38 50%:15	max:105 75%:59 50%:24	max:139 75%:78 50%:32	max:175 75%:96 50%:41	max:209 75%:116 50%:51	max:244 75%:134 50%:60
0.875	max:77 75%:42 50%:14	max:116 75%:64 50%:22	max:154 75%:84 50%:30	max:193 75%:104 50%:39	max:231 75%:124 50%:47	max:270 75%:146 50%:56
1.000	max:84 75%:44 50%:14	max:127 75%:67 50%:21	max:168 75%:91 50%:29	max:211 75%:114 50%:37	max:254 75%:137 50%:45	max:295 75%:159 50%:53

(c) 15° arch inclination: robotic reachability data

Rise-to-Span \ Span [m]	2	3	4	5	6	7
0.125	C:100% fab:131	C:100% fab:148	C:100% fab:160	C:100% fab:164	C:100% fab:161	C:92% fab:146
0.250	C:100% fab:153	C:100% fab:165	C:100% fab:169	C:100% fab:169	C:100% fab:163	C:93% fab:138
0.375	C:100% fab:161	C:100% fab:168	C:100% fab:169	C:100% fab:162	C:100% fab:144	C:72% fab:88
0.500	C:100% fab:164	C:100% fab:169	C:100% fab:161	C:100% fab:143	C:70% fab:93	C:29% fab:42
0.625	C:100% fab:165	C:100% fab:164	C:100% fab:146	C:67% fab:99	C:54% fab:70	C:23% fab:34
0.750	C:100% fab:165	C:100% fab:154	C:73% fab:109	C:56% fab:83	C:45% fab:57	C:20% fab:29
0.875	C:100% fab:164	C:88% fab:132	C:63% fab:95	C:49% fab:71	C:38% fab:48	C:18% fab:25
1.000	C:100% fab:160	C:76% fab:114	C:56% fab:83	C:44% fab:64	C:34% fab:42	C:16% fab:23

(d) 15° arch inclination: robotic support payloads (kg)

Rise-to-Span \ Span [m]	2	3	4	5	6	7
0.125	max:61 75%:39 50%:16	max:103 75%:77 50%:33	max:143 75%:114 50%:59	max:180 75%:151 50%:93	max:220 75%:188 50%:128	max:259 75%:226 50%:164
0.250	max:51 75%:35 50%:18	max:78 75%:58 50%:34	max:104 75%:79 50%:54	max:132 75%:101 50%:74	max:158 75%:121 50%:93	max:184 75%:141 50%:113
0.375	max:51 75%:33 50%:18	max:76 75%:51 50%:30	max:102 75%:70 50%:44	max:127 75%:85 50%:59	max:154 75%:104 50%:73	max:179 75%:121 50%:86
0.500	max:55 75%:34 50%:16	max:82 75%:51 50%:27	max:109 75%:68 50%:39	max:137 75%:85 50%:51	max:164 75%:102 50%:62	max:190 75%:118 50%:73
0.625	max:59 75%:36 50%:16	max:90 75%:53 50%:25	max:120 75%:71 50%:36	max:149 75%:89 50%:46	max:179 75%:107 50%:56	max:209 75%:125 50%:66
0.750	max:66 75%:37 50%:16	max:99 75%:58 50%:25	max:131 75%:77 50%:34	max:165 75%:96 50%:43	max:197 75%:115 50%:53	max:231 75%:133 50%:62
0.875	max:68 75%:42 50%:15	max:102 75%:64 50%:24	max:136 75%:84 50%:34	max:170 75%:103 50%:44	max:204 75%:124 50%:53	max:238 75%:145 50%:62
1.000	max:73 75%:45 50%:16	max:110 75%:68 50%:25	max:146 75%:91 50%:34	max:183 75%:114 50%:44	max:220 75%:137 50%:54	max:256 75%:159 50%:63

(e) 22.5° arch inclination: robotic reachability data

Rise-to-Span \ Span [m]	2	3	4	5	6	7
0.125	C:100% fab:130	C:100% fab:144	C:100% fab:159	C:100% fab:163	C:100% fab:160	C:92% fab:146
0.250	C:100% fab:152	C:100% fab:165	C:100% fab:169	C:100% fab:167	C:100% fab:158	C:91% fab:130
0.375	C:100% fab:161	C:100% fab:168	C:100% fab:165	C:100% fab:155	C:100% fab:134	C:55% fab:69
0.500	C:100% fab:164	C:100% fab:165	C:100% fab:153	C:88% fab:124	C:63% fab:82	C:27% fab:39
0.625	C:100% fab:164	C:100% fab:157	C:90% fab:129	C:64% fab:92	C:50% fab:63	C:22% fab:32
0.750	C:100% fab:162	C:100% fab:147	C:69% fab:100	C:55% fab:77	C:40% fab:50	C:19% fab:27
0.875	C:100% fab:158	C:84% fab:122	C:60% fab:87	C:47% fab:66	C:36% fab:44	C:17% fab:24
1.000	C:100% fab:153	C:72% fab:105	C:52% fab:76	C:41% fab:58	C:31% fab:38	C:15% fab:21

(f) 22.5° arch inclination: robotic support payloads (kg)

Rise-to-Span \ Span [m]	2	3	4	5	6	7
0.125	max:57 75%:37 50%:16	max:95 75%:72 50%:32	max:132 75%:106 50%:56	max:166 75%:140 50%:87	max:202 75%:173 50%:120	max:238 75%:208 50%:153
0.250	max:48 75%:34 50%:18	max:72 75%:55 50%:32	max:97 75%:74 50%:51	max:122 75%:95 50%:70	max:146 75%:113 50%:87	max:170 75%:132 50%:105
0.375	max:47 75%:32 50%:18	max:71 75%:48 50%:29	max:96 75%:66 50%:43	max:119 75%:81 50%:56	max:143 75%:99 50%:70	max:167 75%:116 50%:82
0.500	max:51 75%:33 50%:16	max:77 75%:49 50%:28	max:102 75%:66 50%:39	max:128 75%:83 50%:50	max:153 75%:99 50%:61	max:178 75%:114 50%:72
0.625	max:52 75%:35 50%:16	max:78 75%:52 50%:26	max:104 75%:69 50%:36	max:130 75%:87 50%:46	max:156 75%:104 50%:56	max:181 75%:121 50%:66
0.750	max:56 75%:37 50%:17	max:85 75%:57 50%:27	max:113 75%:76 50%:36	max:141 75%:95 50%:47	max:169 75%:114 50%:57	max:198 75%:132 50%:67
0.875	max:61 75%:42 50%:18	max:92 75%:63 50%:27	max:121 75%:84 50%:38	max:152 75%:103 50%:48	max:182 75%:124 50%:58	max:213 75%:145 50%:69
1.000	max:65 75%:45 50%:18	max:98 75%:68 50%:29	max:129 75%:92 50%:39	max:162 75%:115 50%:50	max:195 75%:138 50%:61	max:227 75%:159 50%:72

TableA.2robotic reachability data (left) and robotic support payloads (right) in planar arch construction with two high-payload robots in fixed positions

(a) 7.5° arch inclination: robotic reachability data

Rise-to-Span \ Span [m]	2	3	4	5	6	7
0.125	C:100% fab:98	C:100% fab:114	C:100% fab:117	C:93% fab:105	C:75% fab:89	C:65% fab:77
0.250	C:100% fab:110	C:100% fab:122	C:100% fab:125	C:90% fab:112	C:72% fab:91	C:60% fab:75
0.375	C:100% fab:114	C:100% fab:126	C:100% fab:132	C:87% fab:104	C:63% fab:70	C:48% fab:51
0.500	C:100% fab:116	C:100% fab:124	C:100% fab:124	C:86% fab:75	C:43% fab:36	C:32% fab:27
0.625	C:100% fab:114	C:100% fab:120	C:100% fab:102	C:40% fab:28	C:29% fab:20	C:25% fab:16
0.750	C:100% fab:112	C:100% fab:108	C:80% fab:68	C:29% fab:17	C:23% fab:13	C:19% fab:11
0.875	C:100% fab:109	C:100% fab:93	C:63% fab:51	C:23% fab:12	C:19% fab:10	C:17% fab:8
1.000	C:100% fab:101	C:78% fab:73	C:53% fab:40	C:20% fab:9	C:16% fab:7	C:14% fab:6

(b) 7.5° arch inclination: robotic support payloads (kg)

Rise-to-Span \ Span [m]	2	3	4	5	6	7
0.125	max:64 75%:40 50%:16	max:108 75%:80 50%:34	max:151 75%:119 50%:61	max:191 75%:159 50%:96	max:232 75%:198 50%:133	max:274 75%:238 50%:172
0.250	max:54 75%:37 50%:19	max:82 75%:61 50%:34	max:109 75%:82 50%:56	max:139 75%:106 50%:77	max:166 75%:127 50%:97	max:194 75%:148 50%:118
0.375	max:53 75%:34 50%:18	max:80 75%:52 50%:30	max:107 75%:72 50%:46	max:134 75%:88 50%:61	max:161 75%:108 50%:75	max:188 75%:126 50%:89
0.500	max:57 75%:34 50%:16	max:86 75%:52 50%:27	max:115 75%:69 50%:39	max:144 75%:87 50%:51	max:173 75%:104 50%:63	max:200 75%:121 50%:74
0.625	max:62 75%:36 50%:15	max:95 75%:54 50%:25	max:127 75%:72 50%:36	max:157 75%:90 50%:45	max:189 75%:108 50%:55	max:220 75%:127 50%:65
0.750	max:70 75%:38 50%:15	max:105 75%:59 50%:24	max:139 75%:78 50%:32	max:175 75%:96 50%:41	max:209 75%:116 50%:51	max:244 75%:134 50%:60
0.875	max:77 75%:42 50%:14	max:116 75%:64 50%:22	max:154 75%:84 50%:30	max:193 75%:104 50%:39	max:231 75%:124 50%:47	max:270 75%:146 50%:56
1.000	max:84 75%:44 50%:14	max:127 75%:67 50%:21	max:168 75%:91 50%:29	max:211 75%:114 50%:37	max:254 75%:137 50%:45	max:295 75%:159 50%:53

(c) 15° arch inclination: robotic reachability data

Rise-to-Span \ Span [m]	2	3	4	5	6	7
0.125	C:100% fab:98	C:100% fab:114	C:100% fab:116	C:91% fab:104	C:75% fab:87	C:65% fab:76
0.250	C:100% fab:110	C:100% fab:121	C:100% fab:124	C:90% fab:107	C:71% fab:86	C:58% fab:71
0.375	C:100% fab:114	C:100% fab:124	C:100% fab:125	C:87% fab:97	C:56% fab:61	C:42% fab:44
0.500	C:100% fab:113	C:100% fab:121	C:100% fab:115	C:77% fab:68	C:35% fab:31	C:28% fab:24
0.625	C:100% fab:112	C:100% fab:115	C:100% fab:98	C:33% fab:24	C:26% fab:18	C:20% fab:14
0.750	C:100% fab:109	C:100% fab:104	C:66% fab:58	C:23% fab:14	C:20% fab:12	C:17% fab:10
0.875	C:100% fab:104	C:79% fab:78	C:54% fab:45	C:20% fab:10	C:16% fab:9	C:14% fab:7
1.000	C:100% fab:98	C:67% fab:65	C:45% fab:35	C:16% fab:8	C:14% fab:7	C:12% fab:6

(d) 15° arch inclination: robotic support payloads (kg)

Rise-to-Span \ Span [m]	2	3	4	5	6	7
0.125	max:61 75%:39 50%:16	max:103 75%:77 50%:33	max:143 75%:114 50%:59	max:180 75%:151 50%:93	max:220 75%:188 50%:128	max:259 75%:226 50%:164
0.250	max:51 75%:35 50%:18	max:78 75%:58 50%:34	max:104 75%:79 50%:54	max:132 75%:101 50%:74	max:158 75%:121 50%:93	max:184 75%:141 50%:113
0.375	max:51 75%:33 50%:18	max:76 75%:51 50%:30	max:102 75%:70 50%:44	max:127 75%:85 50%:59	max:154 75%:104 50%:73	max:179 75%:121 50%:86
0.500	max:55 75%:34 50%:16	max:82 75%:51 50%:27	max:109 75%:68 50%:39	max:137 75%:85 50%:51	max:164 75%:102 50%:62	max:190 75%:118 50%:73
0.625	max:59 75%:36 50%:16	max:90 75%:53 50%:25	max:120 75%:71 50%:36	max:149 75%:89 50%:46	max:179 75%:107 50%:56	max:209 75%:125 50%:66
0.750	max:66 75%:37 50%:16	max:99 75%:58 50%:25	max:131 75%:77 50%:34	max:165 75%:96 50%:43	max:197 75%:115 50%:53	max:231 75%:133 50%:62
0.875	max:68 75%:42 50%:15	max:102 75%:64 50%:24	max:136 75%:84 50%:34	max:170 75%:103 50%:44	max:204 75%:124 50%:53	max:238 75%:145 50%:62
1.000	max:73 75%:45 50%:16	max:110 75%:68 50%:25	max:146 75%:91 50%:34	max:183 75%:114 50%:44	max:220 75%:137 50%:54	max:256 75%:159 50%:63

(e) 22.5° arch inclination: robotic reachability data

Rise-to-Span \ Span [m]	2	3	4	5	6	7
0.125	C:100% fab:97	C:100% fab:113	C:100% fab:116	C:90% fab:103	C:75% fab:86	C:63% fab:74
0.250	C:100% fab:109	C:100% fab:121	C:100% fab:123	C:87% fab:100	C:67% fab:77	C:53% fab:60
0.375	C:100% fab:111	C:100% fab:120	C:100% fab:114	C:85% fab:85	C:47% fab:46	C:37% fab:36
0.500	C:100% fab:111	C:100% fab:113	C:100% fab:102	C:40% fab:35	C:29% fab:24	C:24% fab:20
0.625	C:100% fab:107	C:100% fab:107	C:78% fab:71	C:26% fab:18	C:21% fab:14	C:18% fab:12
0.750	C:100% fab:103	C:94% fab:91	C:58% fab:48	C:19% fab:11	C:16% fab:9	C:13% fab:8
0.875	C:100% fab:100	C:69% fab:65	C:45% fab:36	C:16% fab:9	C:13% fab:7	C:11% fab:6
1.000	C:98% fab:93	C:59% fab:55	C:38% fab:29	C:13% fab:6	C:11% fab:5	C:9% fab:4

(f) 22.5° arch inclination: robotic support payloads (kg)

Rise-to-Span \ Span [m]	2	3	4	5	6	7
0.125	max:57 75%:37 50%:16	max:95 75%:72 50%:32	max:132 75%:106 50%:56	max:166 75%:140 50%:87	max:202 75%:173 50%:120	max:238 75%:208 50%:153
0.250	max:48 75%:34 50%:18	max:72 75%:55 50%:32	max:97 75%:74 50%:51	max:122 75%:95 50%:70	max:146 75%:113 50%:87	max:170 75%:132 50%:105
0.375	max:47 75%:32 50%:18	max:71 75%:48 50%:29	max:96 75%:66 50%:43	max:119 75%:81 50%:56	max:143 75%:99 50%:70	max:167 75%:116 50%:82
0.500	max:51 75%:33 50%:16	max:77 75%:49 50%:28	max:102 75%:66 50%:39	max:128 75%:83 50%:50	max:153 75%:99 50%:61	max:178 75%:114 50%:72
0.625	max:52 75%:35 50%:16	max:78 75%:52 50%:26	max:104 75%:69 50%:36	max:130 75%:87 50%:46	max:156 75%:104 50%:56	max:181 75%:121 50%:66
0.750	max:56 75%:37 50%:17	max:85 75%:57 50%:27	max:113 75%:76 50%:36	max:141 75%:95 50%:47	max:169 75%:114 50%:57	max:198 75%:132 50%:67
0.875	max:61 75%:42 50%:18	max:92 75%:63 50%:27	max:121 75%:84 50%:38	max:152 75%:103 50%:48	max:182 75%:124 50%:58	max:213 75%:145 50%:69
1.000	max:65 75%:45 50%:18	max:98 75%:68 50%:29	max:129 75%:92 50%:39	max:162 75%:115 50%:50	max:195 75%:138 50%:61	max:227 75%:159 50%:72

Appendix B. Computational workflow for the planar arch parametric study

To provide additional information to readers interested in the computational workflow for the planar arch parametric study, we have chosen present a visual schematic of the computational script. This annotated Grasshopper canvas, aims to offer insight into the high-level functionality of the script. See Figures B.17 and B.18 for a schematic of the computational workflow for the reachability and robotic payload analysis respectively. Furthermore, the necessary input data (i.e., arch geometries and reachability maps) are uploaded as supplementary material with this paper. Thus, we are enabling users to recreate the analyses with their own computational processes based using the arch geometries we studied and the reachability maps we generated for the specific robotic setups described in this paper.

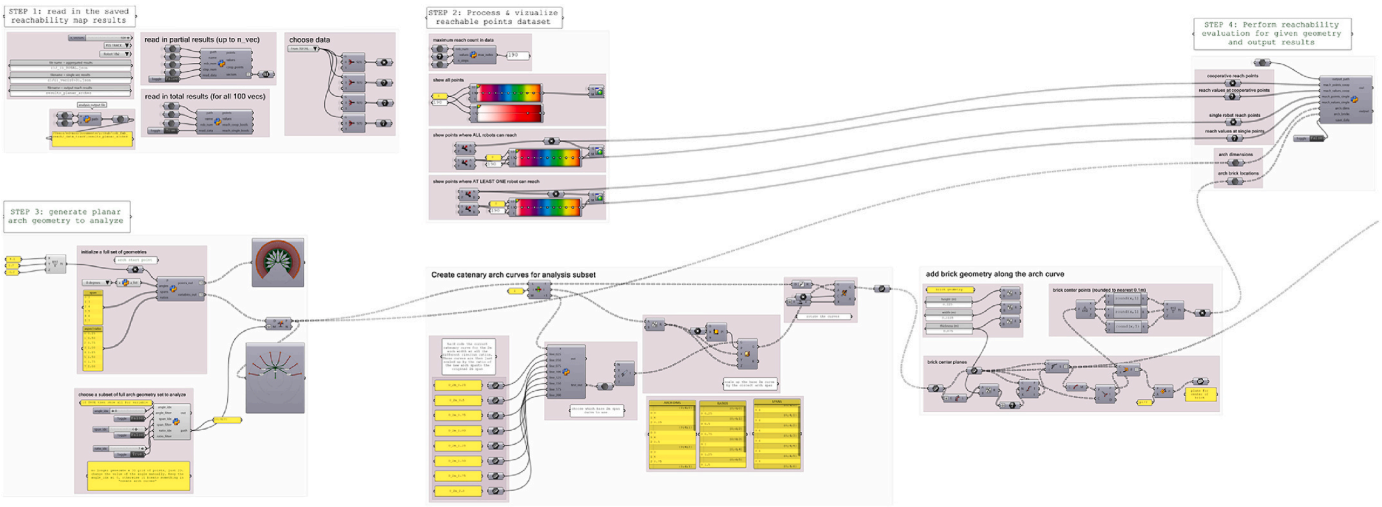

Fig. B.17. High-level computational workflow for the robotic reachability analysis.

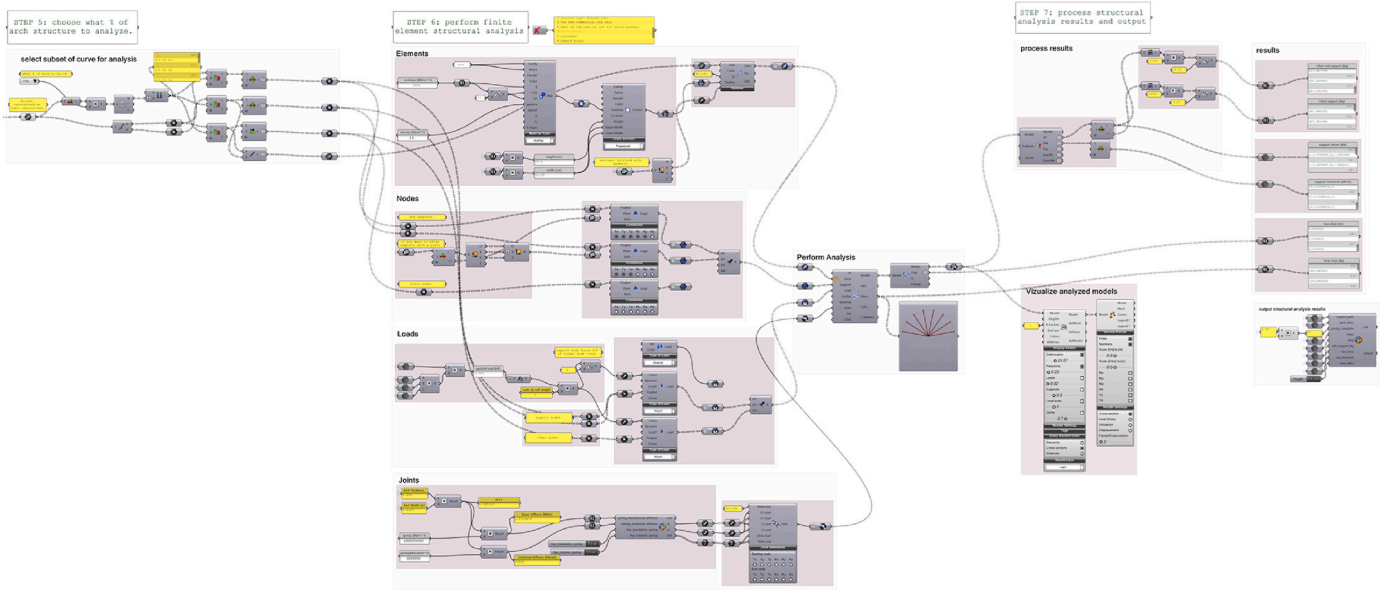

Fig. B.18. High-level computational workflow for the robotic payload analysis.

References

ABB Ltd., 2023. ABB Robotics industrial robots product range. URL. https://search.abb.com/library/Download.aspx?DocumentID=9AKK107992A0209&LanguageCode=en&DocumentPartId=&Action=Launch.

Adam, R., 1764. Ruins of the Palace of the Emperor Diocletian at Spalatro in Dalmatia. Pantianos Classics, London. https://doi.org/10.5479/sil.414240.39088006652358.

Akleman, E., Krishnamurthy, V.R., Fu, C.-A., Subramanian, S.G., Ebert, M., Eng, M., Starrett, C., Panchal, H., 2020. Generalized abeille tiles: topologically interlocked space-filling shapes generated based on fabric symmetries. Comput. Graph. 89, 156–166. https://doi.org/10.1016/j.cag.2020.05.016.

Al Asali, M.W., 2021. Craft-inclusive Construction: Design Strategies for Thin-Tile Vaulting, Ph.D. Thesis. University of Cambridge. https://doi.org/10.17863/CAM.70426.

Al Asali, W., Reynolds, T., Ramage, M., 2021. Bending Parabolas: Formwork for Compression-Only Structures. Georgia Institute of Technology: School of Architecture Symposia, pp. 43–50. https://doi.org/10.35090/gatech/83.

Alkadi, R.M., 2017. The Origin of the Islamic Ribbed Vaults Famed in North Africa and Spain. Universidad Politécnica de Madrid. https://doi.org/10.20868/UPM.thesis.47687. PhD Thesis.

Allen, E., 1979. Pietre di Puglia: Dolmen, trulli e insediamenti rupestri, Adda. ISBN: 978-88-8082-077-2.

Gabinete de Arquitectura, Breaking the Siege. In: Aravena, A. (Ed.), 2016. Reporting from the Front - the Official Catalogue of the 15th Venice Biennale Architecture Exhibition, 1. Marsilio, Venice, Italy, pp. 36–39. ISBN: 978-88-317-2377-0.

Arce, I., 2003. From the diaphragm arches to the ribbed vaults. An hypothesis for the birth and development of a building technique. In: Proceedings of the First

International Congress on Construction History, Madrid, pp. 225–241. ISBN: 84-9728-070-9.
Askarov, S., 2004. Amir temur and Philippe Brunelleschi. URL. https://sanat.orexca.com/2004/2004-3/history_art5/.
Auroville Earth Institute, Auroville Earth Institute, 2022. UNESCO chair earthen architecture. URL. https://www.earth-auroville.com/.
Benvenuto, E., Corradi, M., 1987. La statica delle false volte. In: Architettura in pietra a secco. Atti del 1° Seminario internazionale. Schena Editore, pp. 93–106. ISBN: 978-88-7514-413-5.
Block, P., Bayl-Smith, M., Schork, T., Bellamy, J., Pigram, D., Gramazio, F., Kohler, M., Langenberg, S., 2017. Ribbed tile vaulting: innovation through two design-build workshops. In: Fabricate 2014: Negotiating Design & Making. UCL Press, pp. 22–29. https://doi.org/10.2307/j.ctt1tp3c5w.6.
Brambilla, M.G., 2012. Large scale building techniques in ilkhanid Iran. In: Masons at Work: Architecture and Construction in the Pre-modern World. University of Pennsylvania, p. 18. URL. https://www.sas.upenn.edu/ancient/masons/brambilla.pdf.
Brocato, M., Mondardini, L., 2012. A new type of stone dome based on Abeille's bond. Int. J. Solid Struct. 49 (13), 1786–1801. https://doi.org/10.1016/j.ijsolstr.2012.03.036.
Bruun, E.P.G., Ting, I., Adriaenssens, S., Parascho, S., 2020. Human–robot collaboration: a fabrication framework for the sequential design and construction of unplanned spatial structures. Digit. Creativ. 31 (4), 320–336. https://doi.org/10.1080/14626268.2020.1845214.
Bruun, E.P.G., Pastrana, R., Paris, V., Beghini, A., Pizzigoni, A., Parascho, S., Adriaenssens, S., 2021. Three cooperative robotic fabrication methods for the scaffold-free construction of a masonry arch. Autom. ConStruct. 129, 103803 https://doi.org/10.1016/j.autcon.2021.103803.
Bruun, E.P.G., Adriaenssens, S., Parascho, S., 2022a. Structural rigidity theory applied to the scaffold-free (dis)assembly of space frames using cooperative robotics. Autom. ConStruct. 141, 104405 https://doi.org/10.1016/j.autcon.2022.104405.
Bruun, E.P.G., Adriaenssens, S., Besler, E., Parascho, S., 2022b. ZeroWaste: towards computing cooperative robotic sequences for the disassembly and reuse of timber frame structures. In: Proceedings of the 42nd Annual Conference of the Association for Computer Aided Design in Architecture. Philadelphia, USA, pp. 586–597. URL. http://arks.princeton.edu/ark:/88435/pr1wp9t657.
Bruun, E.P.G., Parascho, S., Adriaenssens, S., 2024a. Cooperative robotic fabrication for a circular economy. In: De Wolf, C., Çetin, S., Bocken, N. (Eds.), A Circular Built Environment in the Digital Age, Circular Economy and Sustainability. Springer, Cham, pp. 129–149. https://doi.org/10.1007/978-3-031-39675-5_8.
Bruun, E.P.G., Besler, E., Adriaenssens, S., Parascho, S., 2024b. Scaffold-free cooperative robotic disassembly and reuse of a timber structure in the ZeroWaste project. Construction Robotics 8 (20), 39. https://doi.org/10.1007/s41693-024-00137-7.
Cappai, S.N., 2003. A hypothesis on a building technique to determine the shape of the Nuragic tholoi. In: Proceedings of the First International Congress on Construction History. Reverte, Madrid, pp. 535–544. ISBN: 84-9728-070-9.
Carneau, P., Mesnil, R., Roussel, N., Baverel, O., 2020. Additive manufacturing of cantilever - from masonry to concrete 3D printing. Autom. ConStruct. 116, 1–16. https://doi.org/10.1016/j.autcon.2020.103184.
Choisy, A., 1871. Note sur la construction des voutes sans cintrage pendant la période byzantine. In: Annales des Ponts Et Chaussées, 1 of 5. Dunod, Paris, pp. 439–449. ISBN: 978-1-391-46827-3.
Choisy, A., 1883. L'Art de bâtir chez les Byzantins. Société anonyme de publications périodiques, Paris. ISBN: 978-88-271-1911-2.
Collins, G.R., 1968. The transfer of thin masonry vaulting from Spain to America. J. Soc. Archit. Hist. 27 (3), 176–201. https://doi.org/10.2307/988501.
Copeland, P.W., 1955. Beehive villages of North Syria. Antiquity 29 (113), 21–24. https://doi.org/10.1017/S0003598X00025503.
CREATE laboratory Princeton, LightVault. URL. https://vimeo.com/467843836.
Davis, L., Rippmann, M., Pawlofsky, T., Block, P., 2012. Innovative funicular tile vaulting: a prototype in Switzerland. Struct. Eng. 90 (11), 46–56. URL. https://www.istructe.org/journal/volumes/volume-90-(2012)/issue-11/research-innovative-funicular-tile-vaulting-a-prot/.
De Wolf, C., Ramage, M., Ochsendorf, J., 2016. Low carbon vaulted masonry structures. Journal of the International Association for Shell and Spatial Structures 57 (4), 275–284. https://doi.org/10.20898/j.iass.2016.190.854.
Deuss, M., Panozzo, D., Whiting, E., Liu, Y., Block, P., Sorkine-Hornung, O., Pauly, M., 2014. Assembling self-supporting structures. ACM Trans. Graph. 33 (6), 1–10. https://doi.org/10.1145/2661229.2661266.
Drew, J., 2017. Formwork for use in the construction of arched structures and method of constructing arched structures. URL. https://patents.justia.com/patent/9828760.
Dyskin, A.V., Estrin, Y., Kanel-Belov, A.J., Pasternak, E., 2003. Topological interlocking of platonic solids: a way to new materials and structures. Phil. Mag. Lett. 83 (3), 197–203. https://doi.org/10.1080/0950083031000065226.
Fantin, M., Ciblac, T., Brocato, M., 2018. Resistance of flat vaults taking their stereotomy into account. J. Mech. Mater. Struct. 13 (5), 657–677. https://doi.org/10.2140/jomms.2018.13.657.
Fathy, H., 1973. Architecture for the Poor: an Experiment in Rural Egypt, nachdr. Edition. Univ. Press, Chicago, Ill. ISBN: 978-0-226-23916-3.
Fisher, C.S., 1924. The Minor Cemetery at Giza. University Museum, Philadelphia. URL. http://www.gizapyramids.org/pdf_library/fisher_minor_cemetery.pdf.
Fitchen, J., 1981. The Construction of Gothic Cathedrals: A Study of Medieval Vault Erection. University of Chicago Press, Chicago. ISBN: 978-0-226-25203-2.
Fraddosio, A., Lepore, N., Piccioni, M.D., 2019. Further refinement of the Corbelling Theory for the equilibrium analysis of corbelled domes. Curved Layer. Struct. 6 (1), 30–40. https://doi.org/10.1515/cls-2019-0003.
Fuentes, P., Huerta, S., 2010. Islamic domes of crossed-arches: origin, geometry and structural behavior. In: 6th International Conference on Arch Bridges, Fuzhou, China, pp. 346–353. ISBN: 978-953-7621-10-0.
Fuentes, P., Huerta, S., 2015. Crossed-arch vaults in late Gothic and early Renaissance vaulting: a problem of building technology transfer. In: Proceedings of the Fifth International Congress on Construction History, Chicago, p. 8. ISBN: 978-1-329-15031-7.
Gabinete de Arquitectura, 2015. Teletón children's rehabilition centerr (second phase). a +u 532 (1). URL. https://au-magazine.com/shop/architecture-and-urbanism/au-201501/.
Gallon, J.-G., 1735. Machines et inventions approuvees par l'Academie royale des sciences, 2. Martin-Coignard-Guerin, Paris. https://gallica.bnf.fr/ark:/12148/bpt6k3476b.
García de Soto, B., Agustí-Juan, I., Hunhevicz, J., Joss, S., Graser, K., Habert, G., Adey, B. T., 2018. Productivity of digital fabrication in construction: cost and time analysis of a robotically built wall. Autom. ConStruct. 92, 297–311. https://doi.org/10.1016/j.autcon.2018.04.004.
Gupta, A., Robb, D., Long, A., Mcpolin, D., Nanukuttan, S., 2016. 'FlexiArch': rapid method of constructing arches. In: Proceedings of the Sixth International Conference on Structural Engineering, Mechanics and Computation. CRC Press, Cape Town, South Africa, pp. 1640–1644. https://doi.org/10.1201/9781315641645-291.
Guzmán Urbina, X., Hernández Hernández, A., San Martín Córdova, I. (Eds.), 2010. Fernando López Carmona: Arquitecto, 50 años de enseñanza, first ed. Colección Arquitectura, Universidad Nacional Autónoma de México, México. ISBN: 978-607-02-0967-3.
Han, I.X., Bruun, E.P.G., Marsh, S., Adriaenssens, S., Parascho, S., 2020. From concept to construction: a transferable design and robotic fabrication method for a building-scale vault. In: Proceedings of the 40th Annual Conference of the Association for Computer Aided Design in Architecture. Online, pp. 614–623. https://doi.org/10.52842/conf.acadia.2020.1.614.
Hanna, A.S., 1998. Concrete Formwork Systems, first ed. CRC Press, Boca Raton. https://doi.org/10.1201/9780203909690.
Huerta, S., 2009. The geometry and construction of byzantine vaults: the fundamental contribution of Auguste Choisy. In: Auguste Choisy (1841-1909): L'architecture et l'art de bâtir. Universidad Politécnica de Madrid, pp. 289–305. ISBN: 978-84-9728-318-2.
Itasca consulting group Inc., 3DEC. URL. https://www.itascacg.com/software/3dec.
Jalia, A., 2017. Innovative Masonry Shell Construction in India's Evolving Building Crafts : A Case for Tile Vaulting, Ph.D. University of Cambridge. https://doi.org/10.17863/CAM.18674.
Ko, C.-H., Kuo, J.-D., 2015. Making formwork construction lean. J. Civ. Eng. Manag. 21 (4), 444–458. https://doi.org/10.3846/13923730.2014.890655.
Kundoo, A., 2014. Wall house. Palimpsest 11, 8–9. https://doi.org/10.5821/palimpsesto.11.3695.
Lab, R.H., 2007. Think Formwork - Reduce Costs, Structure Magazine, pp. 14–16. URL. https://www.structuremag.org/?p=6139.
Lancaster, L.C., 2009. Auguste Choisy and the economics of roman construction. In: Auguste Choisy (1841-1909): L'architecture et l'art de bâtir. Universidad Politécnica de Madrid, pp. 307–328. ISBN: 978-84-9728-318-2.
Lancaster, L.C., 2015a. Complex vault forms of brick. In: Innovative Vaulting in the Architecture of the Roman Empire: 1st to 4th Centuries CE. Cambridge University Press, Cambridge, pp. 70–98. https://doi.org/10.1017/CBO9781107444935.005.
Lancaster, L.C., 2015b. Vaulting tubes. In: Innovative Vaulting in the Architecture of the Roman Empire: 1st to 4th Centuries CE. Cambridge University Press, Cambridge, pp. 99–128. https://doi.org/10.1017/CBO9781107444935.006.
Lassaulx, J.K.v., 1829. Beschreibung des Verfahrens bei Anfertigung leichter Gewölbe über Kirchen und ähnliche Räumen. Journal für die Baukunst 317–330. https://doi.org/10.11588/diglit.19234.35. G. Reimer, Berlin.
Lassaulx, J.K.v., Whewell, W., 1831. Description of a mode of erecting light vaults over churches and similar spaces. In: The Journal of the Royal Institution of Great Britain, 1. John Murray, London, pp. 224–240 (OCLC: 175312420).
Lassure, C., 2009. Building a Drystone Hut: an Instruction Manual, second ed. C.E.R.A.V., Paris. iSBN: 0751-9656.
Loing, V., Baverel, O., Caron, J.-F., Mesnil, R., 2020. Free-form structures from topologically interlocking masonries. Autom. ConStruct. 113, 1–15. https://doi.org/10.1016/j.autcon.2020.103117.
López López, D., Domènech Rodríguez, M., Palumbo Fernández, M., 2014. Brick-topia. the thin-tile vaulted pavilion, Case Studies in Structural Engineering 2, 33–40. https://doi.org/10.1016/j.csse.2014.09.001.
López López, D., Van Mele, T., Block, P., 2016. La bóveda tabicada en el siglo XXI. Inf. Construcción 68 (544), 162. https://doi.org/10.3989/ic.15.169.m15.
Mainstone, R.J., 1969. Brunelleschi's Dome of S. Maria del Fiore and some Related Structures. Trans. N.com. Soc. 42 (1), 107–126. https://doi.org/10.1179/tns.1969.006.
Mecca, S., Dipasquale, L. (Eds.), 2009. Earthen Domes and Habitats: Villages of Northern Syria: an Architectural Tradition Shared by East and West, Progetti Saperi Sentieri. Edizioni ETS, Pisa. ISBN: 978-88-467-2535-6.
Motamedi, M., Mesnil, R., Oval, R., Baverel, O., 2022. Scaffold-free 3D printing of shells: introduction to patching grammar. Autom. ConStruct. 139 https://doi.org/10.1016/j.autcon.2022.104306.
Oates, D., 1970. The excavations at Tell al Rimah, 1968. Iraq 32 (1), 1–26. https://doi.org/10.2307/4199887.
Ochsendorf, J.A., 2013. Guastavino Vaulting: the Art of Structural Tile, first ed. Princeton Architectural Press, New York. ISBN: 978-1-61689-244-9.

Opačić, Z., 2005. Diamond Vaults: Innovation and Geometry in Medieval Architecture. Architectural Association, London. URL. https://eprints.bbk.ac.uk/id/eprint/47690/.

Parascho, S., Han, I.X., Walker, S., Beghini, A., Bruun, E.P.G., Adriaenssens, S., 2020. Robotic vault: a cooperative robotic assembly method for brick vault construction. Construction Robotics 4 (3), 117–126. https://doi.org/10.1007/s41693-020-00041-w.

Parascho, S., Han, I.X., Beghini, A., Miki, M., Walker, S., Bruun, E.P.G., Adriaenssens, S., 2021. LightVault: a design and robotic fabrication method for complex masonry structures. In: Advances in Architectural Geometry 2020. Presses des Ponts, Paris, France, pp. 350–375. https://oar.princeton.edu/handle/88435/pr1s17ss4d.

Paris, V., Pizzigoni, A., Adriaenssens, S., 2020. Statics of self-balancing masonry domes constructed with a cross-herringbone spiraling pattern. Eng. Struct. 215, 10. https://doi.org/10.1016/j.engstruct.2020.110440.

Paris, V., Lepore, N., Bruun, E.P.G., Ruscica, G., Piccioni, M.D., Beghini, A., Parascho, S., Adriaenssens, S., 2021. Robotic construction of a self-balancing glass masonry vault: dem study of stability during construction stages. In: Proceedings of the IASS Annual Symposium 2020/2021, Surrey, pp. 314–325. URL. http://arks.princeton.edu/ark:/88435/pr12n4zh86.

Petralla, S., 2013. Historical vaulted constructions of the Iranian heritage. In: 2nd International Balkans Conference on Challenges of Civil Engineering, Tirana, Albania, pp. 1029–1036. URL. http://dspace.epoka.edu.al/handle/1/1275.

Preisinger, C., Heimrath, M., 2014. Karamba—a toolkit for parametric structural design. Struct. Eng. Int. 24 (2), 217–221. https://doi.org/10.2749/101686614X13830790993483.

Ramage, M., 2007. Guastavino's vault construction revisited. Construction History 22, 47–60. URL. http://www.jstor.org/stable/41613910.

Ramage, M., Hall, T.J., Gatóo, A., Al Asali, M.W., 2019. Rwanda Cricket Stadium: seismically stabilised tile vaults. Structures 18, 2–9. https://doi.org/10.1016/j.istruc.2019.02.004.

Ramírez Ponce, A., Ramírez Melendez, R., 2015. Curves of clay: Mexican brick vaults and domes. In: Williams, K., Ostwald, M.J. (Eds.), Architecture and Mathematics from Antiquity to the Future. Springer International Publishing, Cham, pp. 309–324. https://doi.org/10.1007/978-3-319-00137-1_21.

Ramírez Ponce, A., 2012. Arquitectura propia: Cubiertas de dadrillo recargado. URL. http://ramirezponcearquitecto.blogspot.com/2012/06/arquitectura-propia-cubiertas-de.html.

Reuther, O., 1912. Ocheïdir: Nach Aufnahmen von Mitgliedern der Babylon-Expedition der Deutschen Orient-Gesellschaft. J.C. Hinrichs, Leipzig. https://catalog.hathitrust.org/Record/002639832.

Rippmann, M., Mele, T.V., Popescu, M., Augustynowicz, E., Echenagucia, T.M., Barentin, C.C., Frick, U., Block, P., 2016. Computational design and digital fabrication of a freeform stone shell. In: Advances in Architectural Geometry 2016. Zurich, pp. 344–363. https://doi.org/10.3929/ethz-a-010709080.

Roberti, G.M., Spina, O., 2001. Discrete element analysis on the Sardinian 'Nuaraghe'. In: Historical Constructions: Proceedings of the 3rd International Seminar. Guimarães, Portugal, pp. 719–728. URL. https://api.semanticscholar.org/CorpusID:67839217.

Rossi, C., Fiorillo, F., 2020. The vaults of Umm al-Dabadib: geometric study. Nexus Netw. J. 22 (4), 1063–1080. https://doi.org/10.1007/s00004-020-00532-x.

Rutten, D., 2007. Grasshopper. URL. https://www.grasshopper3d.com/.

Sadeqi, S., Ekhlassi, A., Norouzian-Maleki, S., 2019. An analysis of structural aesthetics in architecture case study: Taj-Ol-Molk Dome, Jˆmeh Mosque of Isfahan, Iran. SN Appl. Sci. 1 (6), 570. https://doi.org/10.1007/s42452-019-0558-5.

Sanders, S.R., Thomas, H.R., 1991. Factors affecting masonry-labor productivity. J. Construct. Eng. Manag. 117 (4), 626–644. https://doi.org/10.1061/(ASCE)0733-9364(1991)117:4(626).

Sanpaolesi, P., 1972. La cupola di Santa Maria del Fiore ed il mausoleo di Soltanieh: Rapporti di forma e struttura fra la cupola del Duomo di Firenze ed il mausoleo del Ilkhan Ulgiaitu a Soltanieh in Persia. Mitt. Kunsthist. Inst. Florenz 16 (3), 221–260. https://doi.org/10.11588/mkhi.1972.3.54269.

Simon, J., Bagi, K., 2016. Discrete element analysis of the minimum thickness of oval masonry domes. Int. J. Architect. Herit. 10 (4), 457–475. https://doi.org/10.1080/15583058.2014.996921.

Talaverano, R.M., Perez de los Rios, M.C., Senent-Dominguez, R., 2012. Late German Gothic methods of vault design and their relationships with Spanish ribbed vaults. In: Proceedings of the Fourth International Congress on Construction History, Paris, pp. 83–90. ISBN: 978-2-7084-0929-3.

Vitti, P., 2021. Brick vaulting without centering in the mediterranean from antiquity to the Middle ages. In: History of Construction Cultures, 1. CRC Press, London, pp. 119–125. https://doi.org/10.1201/9781003173359-16.

von Pilgrim, C., Mueller, W., el Bialy, M., 2011. Report on the Eleventh Season of the Joint Swiss-Egyptian Mission in Syene/Old Aswan (2010/2011). Tech. rep., Swiss Institute of Architectural and Archaeological Research on Ancient Egypt, Cairo. URL. https://www.researchgate.net/publication/353043420_Report_on_the_17th_Season_of_the_Joint_Swiss-Egyptian_Mission_in_Syene_Old_Aswan_20162017.

Wang, Z., Song, P., Isvoranu, F., Pauly, M., 2019. Design and structural optimization of topological interlocking assemblies. ACM Trans. Graph. 38 (6), 1–13. https://doi.org/10.1145/3355089.3356489.

Wendland, D., 2007. Traditional vault construction without formwork: masonry pattern and vault shape in the historical technical literature and in experimental studies. Int. J. Architect. Herit. 1 (4), 311–365. https://doi.org/10.1080/15583050701373803.

Whewell, W., 1830. Architectural Notes on German Churches; with Remarks on the Origin of Gothic Architecture. Cambridge University Press, Cambridge. ISBN: 978-1-108-05176-7.

Woolley, L., 1929. Ur of the Chaldees: a Record of 7 Years of Excavation, first ed. Ernest Benn, London. ISBN: 0-9876759-2-3.

Wu, K., Kilian, A., 2018. Robotic equilibrium: scaffold free arch assemblies. In: Proceedings of the 38th Annual Conference of the Association for Computer Aided Design in Architecture. Mexico City, pp. 342–349. https://doi.org/10.52842/conf.acadia.2018.342.

Wu, K., Kilian, A., 2020. Designing compression-only arch structures using robotic equilibrium assembly. In: Proceedings of the Design Modelling Symposium, Berlin 2019, pp. 608–622. https://doi.org/10.1007/978-3-030-29829-6_47. Berlin.

Zabrana, L., 2018. The nubian Mudbrick vault. A Pharaonic building technique in Nubian village dwellings of the early 20th century. In: The Arts of Making in Ancient Egypt. Voices, Images, and Objects of Material Producers 2000–1550 BC. Sidestone Press, Leiden, pp. 273–284. ISBN: 978-90-8890-523-0.